U-Pb geochronology of variscan granitoids from the Moroccan Meseta (Northwest Africa): tectonic implications

Francis Chopin, Rémi Leprêtre, Mohamed El Houicha, Anne-Sophie Tabaud, Karel Schulmann, Jitka Míková, Jocelyn Barbarand, Ryma Chebli

U–Pb geochronology of variscan granitoids from the Moroccan Meseta (Northwest Africa): tectonic implications

Francis Chopin[1,2], Rémi Leprêtre[3], Mohamed El Houicha[4], Anne-Sophie Tabaud[2], Karel Schulmann[1,2], Jitka Míková[5], Jocelyn Barbarand[6], Ryma Chebli[1,2]

[1] Université de Strasbourg, CNRS, ITES UMR 7063, 5 rue René Descartes, 67084 Strasbourg Cedex, France

[2] Centre for Lithospheric Research, Czech Geological Survey, Klárov 3, 11821 Prague, Czech Republic

[3] CY Cergy Paris Université, Département Géosciences et Environnement (GEC), 1 rue Descartes, 95000 Neuville, Oise Cedex, France

[4] Département de Géologie (LGG), Faculté des Sciences, Université Chouaïb Doukkali, BP.20, 24000, El Jadida, Morocco

[5] Laboratories of the Czech Geological Survey, Geologická 6, Prague, Czech Republic

[6] Université Paris-Saclay, CNRS, GEOPS UMR 8148, Rue du Belvédère, 91405 Orsay Cedex, France

KEY WORDS

U–Pb zircon geochronology, granitoids, Moroccan Meseta, Variscan belt

ABSTRACT

This paper present new U–Pb geochronological data (LA-ICP MS on zircon) of granitoids from the Moroccan Meseta Variscan belt. Zircons from the Oulad Ouaslam granodiorite in the Jebilet massif in the Western Meseta highlight a peak of magmatic activity at 335.2 ± 0.8 Ma. In the Eastern Meseta, the ages obtained from several granitoids facies from the High Moulouya magmatic complex restrained its magmatic activity to the early Visean: 339.6 ± 1.9 Ma for the Perdreaux granite, 337 ± 1.6 Ma for the calc-alkaline «grey» granite and 343.1 ± 1.2 Ma for the El Hassir granodiorite. Similar late Tournaisian – early Visean ages were obtained for the Zekarra granodiorite (348.1 ± 2.3 Ma) and the Merguechoum granite (345.2 ± 2.8 Ma) in the Horsts belt. This pre-orogenic Eovariscan magmatic activity is contemporaneous with the opening of early Carboniferous intracontinental basins in the whole Northwest Africa but its relationship with Eovariscan deformation typifying the Eastern Meseta remains temporally

unclear. Then, the late Carboniferous ages of 308.2 ± 2.7 Ma obtained for the Beni Snassen monzogranite, 303.5 ± 1.7 for the Tanncherfi granodiorite and 305.2 ± 1.4 for the Boudoufoud granite in the Horsts belt show that they all are synchronous with the main late Carboniferous convergent Variscan event in Northwest Africa. This tectonic and magmatic tempos contrast with the one described in the European Variscan belt, where the syn-collisional magmatism forms coevally with the Northwest African Eovariscan event, re-interpreted as a possible extensional event. We proposed that the early Carboniferous intracontinental basins and magmatism in Northwest Africa are due to the propagation of the Paleotethys ocean within the Gondwana continent. In contrary, the late Carboniferous – early Permian tectono-magmatic activity could reflect the docking of the east Gondwana margin with the Iberian branch of the European Variscan belt.

1. INTRODUCTION

The southwest tract of the Palaeozoic Variscan belt remains difficult to follow since it was split between North America and Northwest Africa during the opening of the Central Atlantic Ocean (Martínez-Catalán et al., 2021; Fig. 1). In Northwest Africa, several West African Craton (WAC) derived crustal units constituted the northern Gondwana margin during pre-late Carboniferous times (Michard et al., 2010). These units were in Morocco and Algeria affected by Variscan Paleozoic deformation. Regardless of the Paleozoic basement of the allochthonous internal zones of the Cenozoic Rif-Tell belt, the Morocco Variscan belt is made up of three major fault-bounded crustal units, the Anti-Atlas domain to the south, the Meseta domain in the centre divided into the Western and Eastern Meseta and the Sehoul Block in the north (Fig. 1). The southerly Anti-Atlas domain represents a classical fold-and-thrust belt, the Meseta domain further north corresponds to an internal part of the Northwest African Variscan orogen with unclear affinity to the main European Variscan belt (Hoepffner et al., 2005, 2006; Simancas et al., 2005, 2009; Michard et al., 2010; Martínez-Catalán et al., 2021). In its northernmost part, the exotic Sehoul Block records pre-Upper Devonian orogenic event (e.g. Tahiri et al., 2010).

The geodynamic evolution of the two Meseta sub-domains is contrasted from Upper Devonian to late Carboniferous. In the Eastern Meseta and in the southeastern part of the Morocco Massif Central (MMC) in the Western Meseta, the main compressional deformation (the earliest Variscan phase in the Moroccan Meseta, see Allary et al., 1976) is thought to happen as soon as the Tournaisian-Visean (360–330 Ma) during the so called Eovariscan phase (Hoepffner et al., 2005; Michard et al. 2010; Accotto et al., 2020) while in the major part of the Western Meseta the main compressive event began later, possibly during late Bashkirian-Moscovian (320–305 Ma) (Chopin et al., 2014; Wernert et al., 2016; Delchini et al., 2018; Essaifi et al. 2021). This second event also affected the Eastern Meseta. In the Meseta, the heterogeneous development in space and time of a network of sedimentary basins occurred

from Upper Devonian to early Pennsylvanian, generally related to an extensional deformation (Piqué, 1979; Bouabdelli, 1989; Beauchamps et al., 1991; Tahiri, 1992; Berkhli et al.,1993, 2000; Michard et al., 2008; Becker & El Hassani, 2020; Becker et al., 2021).

Late Paleozoic magmatism is almost absent in the Anti-Atlas, which only shows the controversial presence of dykes, sills and laccoliths (either Devonian or Permian in age, see Pouclet et al. [2017] and Najih et al. [2019], respectively). In contrary, the tectono-thermal evolution of the Moroccan Meseta is characterized by abundant intrusion of granitoids. They outcrop mainly in the Western Meseta in the MMC, the Rehamna, the Jebilet, and the Western High Atlas (WHA) massifs (Fig. 1). In the Eastern Meseta, the granitoid intrusions outcrop mainly in the High Moulouya (Aouli-Mibladen and Boumia inliers in the literature), Tazekka, Debdou-Mekkam and the Horsts belt up to the Tiffrit-Saïda massif (e.g. Gasquet et al., 1996; Amenzou et al., 2001; El Hadi et al., 2003; Remaci-Benaouda, 2005). The Meseta shows dominantly plutonic felsic magmatism with more prominent gabbroic sills, basaltic, andesitic and felsic lavas in the Western Meseta (Michard et al., 2010). Their ages, obtained with various methods (Rb–Sr isochron on whole rocks and minerals, K–Ar, $^{40}Ar/^{39}Ar$, U–Pb), are spreading over 100 Ma covering almost the entire Carboniferous and the early Permian (Tisserant, 1977; Clauer et al. 1980; Mrini et al., 1992; Gasquet et al., 1996; Oukemeni et al., 1995; Ajaji et al., 1998; Baudin et al., 2001, 2003; Cailleux et al., 2001; Essaifi et al., 2003; Chopin et al., 2014; Cheilletz et al, 2015; Rossi et al., 2016, 2017; Aït Lahna et al., 2018; Ettachfini et al., 2018; Delchini et al., 2018; Fekkak et al., 2018; Domeier et al., 2021; Hadimi et al., 2021). So far only one Upper Devonian age was reported from granitoids intruding deformed Cambrian rocks from the Sehoul Block (LA–ICP–MS U–Pb on zircon, Tahiri et al., 2010).

Since the work of El Hadi et al. (2003, 2006) four magmatic periods are traditionally distinguished in the Meseta at ca. 330, 320–300, 290–270 and 270–260 Ma. However, Ikenne et al. (2017) recently proposed that only two major's magmatic periods exited: a late Devonian

– Mississippian and a Pennsylvanian to Permian events. In the Western Meseta, continuous effusive magmatism is known from the Upper Devonian to the end of Serpukhovian (Namurian) with largely documented plutonic activity in the Jebilet and Rehamna massifs (Hoepffner, 1982; Kharbouch, 1994; Essaifi et al., 2014; Delchini et al., 2018; Aït Lahna et al., 2018). This early magmatic activity, contemporaneous with the formation of Upper Devonian – early Carboniferous basins is well established. In contrast, in the Eastern Meseta and south-eastern MMC, the spatiotemporal relationship between this activity and (1) the Upper Devonian – early Carboniferous Eovariscan phase (the earliest Variscan phase of the Meseta) and (2) the development of the late Visean – early Westphalian basins of the Eastern Meseta is highly controversial (Allary et al., 1976; Bouabdelli, 1989; Diot & Bouchez, 1991; Huvelin, 1992; El Mouraouah, 1993; Filali et al., 1999; Hoepffner, 1987; Oukemini et al. 1995; Ajaji et al., 1998; Ben Abbou et al., 2001; El Hadi et al. 2003, 2006; Hoepffner et al., 2005; Michard et al., 2010; Accotto et al., 2020; Lahfid et al., 2019; Leprêtre et al., 2020). Then, the second magmatic activity seems prominent in all places for example in the Western High Atlas (Gasquet et al. 1992, Fekkak et al., 2018) in the Rehamna (Chopin et al, 2014) and the Jebilet massifs (Mrini et al., 1992), in the Morocco Massif Central (Chèvremont et al., 2001; Baudin et al., 2001; Marcoux et al., 2015; Rossi et al., 2016, 2017) or in the Eastern Meseta (Mrini et al., 1992; Oukemeni et al., 1995; Remaci-Benaouda, 2005).

The integration of these two magmatic pulses within the tectonic evolution of the whole Meseta domain is based on the correct determination of the geochronological ages and the significance of the successive tectonic events. However, the existing geochronological dataset represents a first order pitfall for any interpretation of the Meseta geodynamic evolution. This is because most of the magmatic rocks were dated using Rb–Sr method (whole rock or minerals), which may provide false younger ages compared to other more robust methods such as U–Pb geochronology on zircon.

In order to obtain robust data for the age of granitic massifs of the Moroccan Meseta, we provide new LA–ICP–MS U–Pb in-situ zircon ages obtained on granitic samples from the High Moulouya massif and the Horsts belt in the Eastern Meseta and from the Jebilet massif in the Western Meseta. These new ages combined with existing robust U–Pb ages and $^{40}Ar/^{39}Ar$ cooling ages, are used to revise the magmatic history of this domain. Our results from the Western Meseta support the pre-existing data. Those from the eastern Meseta allow for the first time to formally characterize, apart from the Permian age activity, the existence of an important Tournaisian to early-mid Viséan plutonic activity previously identified only in one massif of the High Moulouya magmatic complex (333± 2 Ma, U–Pb, Oukemeni et al. [1995]) and at Tanncherfi (344 ± 6 Ma, Rb–Sr, Ajaji et al. [1998]). This activity would then be synchronous with that of the Western Meseta, but it is within the range accepted for the early Eovariscan so-called compressive phase, and the minimum age of initiation and development of the Carboniferous basins in the Eastern Meseta. Altogether it enables us to discuss geodynamic implications of the magmatic pulses at the scale of the Meseta. Finally, the new tectono-magmatic scheme is correlated with magmatic pulses and related tectonic events affecting the Iberian and southern French parts of the non-cylindrical Variscan belt. This correlation allows proposing a new model of geodynamical evolution of southern branch of the Variscan belt.

2. GEOLOGICAL SETTING

In the Meseta, the Upper Devonian – early Carboniferous Eovariscan tectonic and magmatic activity is generally interpreted as an early expression of suprasubduction event (e.g. Kharbouch et al., 1985; Boulin et al., 1988; Roddaz et al., 2002; Michard et al., 2010; Essaifi et al., 2014) despite the fact that corresponding oceanic suture was not found (Hoepffner et al., 2005). Deformation associated with this event was observed mainly in the Eastern Meseta. It is characterized by low-angle greenschist facies sub-horizontal foliation and sometimes recumbent folds affecting pre-Carboniferous sequences unconformably covered by mostly

Visean intracontinental sediments. These sediments alternate with intraformational bimodal volcanic sills and lava flows which are generally sub-alkali basaltic in the Western Meseta and more andesitic to rhyolitic in the Eastern Meseta (e.g. Kharbouch, 1994). The basins and their basement are sometimes intruded by carboniferous granitic plutons, e.g. in the Jebilet (Essaifi et al., 2014; Delchini et al., 2018) and in the High Moulouya (Oukemeni et al., 1995) massifs. In the Western Meseta, the main compressive Variscan phase is restricted to late Carboniferous (Westphalian in Michard et al., 2010). It is characterized by low grade metamorphism locally reaching the staurolite zone in the Rehamna and Jebilet massifs (Wernert et al., 2016; Delchini et al., 2018). This event is associated with the emplacement of numerous calc-alkaline granitoids in both Meseta (e.g. Ikenne et al., 2017). Finally, early Permian deformation and low-grade metamorphism (e.g. Michard et al., 2010; Chopin et al., 2014; Delchini et al., 2018; Essaifi et al., 2021) are associated with the emplacement of late to post Variscan alkaline magmatism together with the formation of Permian basins (Domeier et al., 2021; Hadimi et al., 2021). Geochemical studies suggest that all these granitoids correspond to mantle derived magmas assimilating continental crust (El Hadi et al., 2006).

Below are synthetized geological and geochronological data from three specific regions which represent the two contrasting tectonic domains in the frame of Morocco Variscides: the Jebilet massif in the Western Meseta, and the High Moulouya massif and the Horsts belt in the Eastern Meseta.

2.1. Jebilet massif

The Jebilet massif in the Western Meseta (e.g. Huvelin, 1977; Bordonaro et al., 1979; Izart et al., 1997; Essaifi et al., 2014) exposes an Upper Devonian – early Carboniferous basin (Huvelin, 1977; Bordonaro et al., 1979) filled by sedimentary and volcanic deposits, which are intruded by several granitoid bodies. The basin is then deformed during late Carboniferous – early Permian (Fig. 2a, Delchini et al., 2018). It is divided into the western Sarhlef and the

eastern Kharrouba series (Huvelin, 1977). Bordonaro et al. (1979) and Beauchamp (1984) proposed that these two formations are laterally equivalent. The Sarhlef serie comprises mainly black shales and sandstones intercalated with volcanoclastics and bimodal sills. Palynostratigraphic age of the black shales has been bracketed at late Visean (Asbian) (Moreno et al., 2008; Playford et al., 2008), but Bordonaro et al. (1979) do not exclude that the serie might be as old as the Tournaisian. Recently, older biostratigraphic ages up to the Frasnian to late Famennian have been proposed from metamorphosed conodonts of the Sarhlef serie (Lazreq et al., 2021). The Kharrouba serie is made of middle to late Visean black shales evolving to turbidites (Izart et al., 1997, revised by Cózar et al., 2020; Becker et al., 2021).

Bimodal magmatism is common within the Sarhlef formation. Mafic sills and dykes (dolerites, gabbros) and rare basaltic lavas have tholeiitic to transitional affinity of mantle origin, whereas felsic ones (rhyolites, granitoids) are alkaline (e.g. Essaifi et al., 2014). Volcanism and associated hydrothermal alteration have been dated at ca. 330.8 ± 1.1 Ma and 331.7 ± 7.9 Ma ($^{40}Ar/^{39}Ar$ on sericite; Marcoux et al., 2008). The small Koudiat Bouzlaf, Koudiat Hamra and Koudiat Kettara felsic plutons have been dated at 330.5 $^{+0.68}_{-0.83}$ Ma (U–Pb ID-TIMS on zircon; Essaifi et al., 2003), 345 ± 2 Ma (LA-ICP-MS on zircon, Delchini et al., 2018) and 346.1 ± 2.7 Ma (SHRIMP on zircon, Aït Lahna et al. 2018), respectively. Similarly, mafic (gabbroic) intrusions have been dated at 348.5 ± 2.6 Ma (Gour es Safra), 343.6 ± 2.6 Ma (Koudiat Kettara) and 336.4 ± 2.9 Ma (Koudiat Arhil) by Aït Lahna et al. (2018) (SHRIMP on zircon). Then, a plutonic complex formed by the Oulad Ouaslam, Tabouchent-Bamega and the smaller Bramram granitoids intrudes both the Sarhlef and Kharrouba formations. The main intrusions were first dated at 319 ± 10 Ma (Tisserant, 1977) and 327 ± 4 Ma (Mrini et al., 1992) using Rb-Sr isochrones, whereas the small late orogenic leucogranites (Bramram intrusion) were dated at ca. 295 Ma (Tisserant, 1977; Mrini et al., 1992). More recently, individual intrusions were dated by Delchini et al. (2018) giving ages of 337 ± 5 Ma, 343 ± 7 Ma, 344 ±

3 Ma and 348 ± 8 Ma for the Oulad Ouaslam, 346±10 Ma and 336 ± 4 Ma for Tabouchent, and 337 ± 4 Ma and 358 ± 7 Ma for the Bamega intrusions (LA-ICP-MS on zircon, Table 1). Based on a structural analysis of intrusions and host rocks, Boummane & Olivier (2007) proposed that the main Oulad Ouaslam intrusion was emplaced as a laccolith during the Late Carboniferous orogenic contraction. The HT–LP conditions of andalusite-cordierite mica schists developed in the aureole of those intrusions (Fig. 2a) have been bracketed between 613 ± 12 °C and 625 ± 25 °C at 2–4 kbar (Delchini et al., 2016). Roof pendants of the intrusion are represented by sillimanite mica schists for which P-T estimates were not estimated (Chemsseddoha, 1986), whereas cordierite-bearing metapelitic xenoliths were equilibrated at ca. 750°C and 3.5 kbar (Bouloton et al., 1991; Bouloton, 1992; Bouloton & Gasquet, 1995). Post orogenic quartz-monzodiorite dykes (Bouloton et al., 2019) dated at ca. 240 Ma (Youbi et al., 2001; Dostal et al., 2005) contain various crustal xenoliths with igneous zircons showing concordant ages at 280–328 Ma, ca. 540–615 Ma, 700 Ma and ca. 2000 Ma together with metamorphic rims at ca. 288–300 Ma (U–Pb, Dostal et al., 2005). This was interpreted as synchronous high-grade metamorphism and formation of S-type granitic magmatism during late Carboniferous – early Permian whereas inherited older ages are compatible with the presence of a West African Craton basement bellow the Paleozoic cover (Dostal et al., 2005).

2.2. High Moulouya massif

The High Moulouya massif (Aouli-Mibladen and Boumia Paleozoic inliers) in the Eastern Meseta (Emberger, 1965; Hoepffner, 1987, El Mouraouah, 1993; Diot & Bouchez, 1989, 1991; Oukemeni & Bourne, 1993; Oukemeni et al, 1995; Filali et al., 1999; Elabouyi et al., 2019) is made of large felsic plutonic bodies intruding metasandstone, metapelite and volcanic sequence affected by contact metamorphism (Fig. 2b, Filali et al., 1999; Elabouyi et al., 2019). The age of the country rocks is attributed to the Cambro–Ordovician (Hoepffner, 1978), but Michard et al. (2008) do not preclude a younger Upper Devonian age.

Four magmatic units (Fig. 2b) were described in the Aouli-Mibladen inlier (Emberger, 1965; Rosé, 1987; Oukemeni & Bourne, 1993; El Mouraouah, 1993; Elabouyi et al., 2019): (1) the mafic to intermediate calc-alkaline to sub-alkaline El Hassir granodiorite; (2) the calc-alkaline metaluminous "grey" granite also called "main" granite; (3) the alkaline peraluminous "pink" granite; and (4) the cordierite-garnet bearing anatectic granites (Fig. 2b). The massif shows two other types of intrusive rocks: (1) isolated peraluminous two-mica "Perdreaux" and "Poulet" granites (Fig. 2b); (2) small gabbro-diorite intrusions NE of the El Hassir granodiorite (Elabouyi et al., 2019). The former type corresponds to leucocratic cordierite±garnet bearing granite containing various xenoliths. Finally, all the intrusions and their country rocks are cut by several meter-scale aplitic and cordierite-muscovite bearing microgranitic dykes.

Available geochronological ages from the intrusions are from Clauer et al. (1980) and Oukemeni et al. (1995) who used Rb–Sr isochrones and U–Pb ID–TIMS technique on zircon, respectively (Table 1): the El Hassir granodiorite was dated at 347 ± 17 Ma (Rb–Sr) and 333 ± 2 Ma (U–Pb), the "pink" granite at 329 ± 6 Ma (Rb–Sr), the "grey" granite at 319 ± 6 Ma (Rb–Sr) and 319 ± 1.5 Ma (U–Pb), and finally, late pegmatites were dated at ca. 310 Ma (Rb–Sr) and microgranites and aplites at 302 ± 3 Ma (Rb–Sr). Clauer et al. (1980) obtained also an age of 368 Ma (Rb–Sr) for the surrounding metamorphosed schists but its signification remains unclear (Filali et al., 1999).

Recumbent asymmetric folds of the country rocks are associated with a sub-horizontal metamorphic foliation S1, E–W stretching lineation and kinematic indicators compatible with a top-to-the-west sense of shear (Hoepffner, 1987, 1994) although Vauchez (1976) favour an opposite sense of shear as in the adjacent Debdou-Mekkam inliers (Accotto et al.,2020). This deformation shows an evolution from oblate to prolate strain in a ductile shear continuum and was interpreted as a result of contractional or extensional deformation related to the synchronous emplacement of the granitoids (Hoepffner, 1987, 1994; Diot & Bouchez, 1989;

1991; El Mouraouah, et al., 1993; Houari, 2003). A second episode was responsible for the development of open, roughly E–W striking upright folds with S2 axial planar cleavage and formation of two structural domes (Emberger, 1965; Hoepffner, 1987). In contrary, Filali et al. (1999) proposed that all the deformation and metamorphism are only caused by the emplacement of the granitoid bodies. The HT–LP metamorphism associated with the development of the S1 and S2 foliations varies from the muscovite zone to the sillimanite zone (Fig. 2b) when approaching the intrusions (450–650° C and 2–4 kbars; El Mouraouah et al., 1993; Filali et al., 1999). Recent petrological analysis from cordierite-garnet bearing anatectic granites permits to estimate the condition of the dehydration melting at 830–870 °C and 6 kbars, with the chemistry of some garnet inner cores suggesting an inherited metamorphism event prior to the partial melting processes (Elabouyi et al., 2019).

2.3. Horsts belt

North-east of the High Moulouya massif, numerous Palaeozoic inliers outcrop below the Mesozoic-Cenozoic sedimentary cover (Lucas, 1952; Guardia, 1975; Hoepffner, 1987), namely the Debdou-Mekkam massif, and the Horsts belt up to the Oujda Mountains and the Algerian High plateaus (Traras, Tiffrit-Saïda) (Fig. 1 and Fig. 2c).

The Ordovician to Carboniferous sedimentary succession shows the occurrence of a regional late Visean unconformity as in the nearby Tazekka massif (Hoepffner, 1987). Based on biostratigraphy, the youngest sediments below the unconformity are mid to Upper Devonian (possibly earliest Tournaisian) in the Debdou-Mekkam massif (Marhoumi et al., 1983; Marhoumi & Rauscher, 1984), Devonian in the Jerada-Oujda area (Torbi, 1996) and early to mid (?) Devonian in Tiffrit-Saïda and Ghar Rouban (Lucas, 1952; Bougara, 2013; Bougara et al., 2017). This is confirmed by the maximum deposit ages (ca. 370 Ma) given by detrital zircons in the Debdou-Mekkam massif (Accotto et al., 2020). In some massifs, volcano-clastic series have been described on top of the unconformity, (Owodenko, 1976; Médioni, 1980) and

dated to the late Visean based on biostratigraphy (Chalot-Prat & Vachard, 1989; Huvelin & Mamet, 1989; Berkhli et al., 1993; Aretz et al., 2010). In the Jerada inlier, the sedimentation continued up to the Moscovian-Kasimovian (Wespthalian C in Desteucq et al. [1988]).

A synschistose deformation below the unconformity has been attributed to an early tectonic phase generally suggested to represent an Eovariscan event (Hoepffner, 1987; Hoepffner et al., 2005, 2006). The metamorphism related to this phase does not exceed greenschist facies (Hoepffner, 1987; Chegham, 1985). Later, the Variscan event s.s., developed during the late Carboniferous up to the early Permian (Michard, 1976; Hoepffner, 1987; Michard et al., 2008, 2010). It is evidenced by ENE–WSW striking upright folds visible in the Horsts belt (Torbi, 1996; Lucas, 1952), in the Debdou-Mekkam massif (Desteucq & Hoepffner, 1980; Accotto et al., 2020), in the Jerada inlier (Owodenko, 1976; Er-Raji, 1997) and below the Mesozoic-Cenozoic cover between the Horsts belt and the Eastern High Atlas (seismic image in Er-Raji, 1997; Taki, 2012). The age of this deformation, mostly inferred from the age of the younger deposit it affects is (syn-) to post-Moscovian (Owodenko, 1946; Desteucq & Hoepffner, 1980; Torbi, 1996; Er-Raji, 1997).

With the exception of the Tiffrit plutonic massif in Algeria which was dated at 297 ± 1 Ma using U–Pb zircon method (Table 1; Remaci-Benaouda, 2005), all ages in this region were obtained from Rb-Sr whole-rock isochrons. The Zekkara intrusions were dated at 287 ± 8 Ma (Mrini et al., 1992) and 284 ± 11 Ma for late calc-alkaline intrusions (Andriès & Benjamin, 1994), the Tanncherfi intrusive complex gave two contrasting ages: 286 ± 10 Ma (Rafi, 1988 in Mrini et al., 1992) and 344 ± 6 Ma (Ajaji et al., 1998) and the smallest Taghilesset and Merguechoum intrusions gave ages of 328 ± 19 and 321 ± 15 Ma (Mrini et al., 1992), respectively. North of Oujda in the Beni Snassen massif, Mrini et al. (1992) proposed an age of 247 ± 7 Ma for a granodiorite. West of Taourirt, a pluton from the Boudoufoud inlier was dated

at 259 ± 11 Ma (Mrini et al., 1992). The Alouana (Debdou-Mekkam massif), Jerada and Soulouina granite intrusions are giving a whole-rock isochron at 284 ± 7 Ma (Tisserant, 1977).

3. LA-ICPMS U–Pb zircon geochronology

3.1. Samples

A medium-grained two-mica granodiorite showing poorly sericitized feldspars from the Oulad Ouslam intrusion has been sampled in the Jebilet massif (J13A, Fig.2). The petrology and geochemistry of this peraluminous, calc-alkaline intrusion are presented in Essaifi et al. (2014). Then, three intrusives rocks were sampled in the High Moulouya massif (Fig. 2): the calc-alkaline "grey" granite (M14), the El Hassir granodiorite (M13A) and the Perdreaux two-mica granite (M11) as defined by Emberger (1965). The sample M14 is a medium-grained biotite granite with Kfs and quartz phenocryst, the sample M13A is a medium-grained mesocratic hornblende granodiorite and the sample M11 is a fine to medium grained two-mica granite. Detailed petrological and geochemical data from these calc-alkaline intrusions can be found in Oukemeni and Bourne (1993). The El Hassir granodiorite and "grey" granite are metaluminous, whereas the Perdreaux two-mica granite is peraluminous (Oukemeni and Bourne, 1993). Finally, five plutonic bodies were sampled in the Horsts belt (Fig. 2): the monzogranite of Beni Snassen (J6-1, after Ruíz Reig [2001] in Berkane geological map and Chaïeb [2004] in Ahfir geological map), the amphibole-bearing granodiorite of Zekkara, NE to the Jerada inlier (J4-1, Andriès & Benjamin, [1994] in Beni-Oukil geological map), the main biotite-granodiorite facies of Tanncherfi (J4-7, Ajaji et al., 1998), the enclave-bearing amphibole granite of Merguechoum (J5-2, Muratet, [1994] in Taourirt geological map) and a biotite-granite facies in the Boudoufoud massif (J5-1, Mrini et al., 1992; Rosé 1987). These intrusions from the Horsts belt are calc-alkaline (El Hadi et al., 2000, 2006), and either peraluminous (Boudoufoud, Beni Snassen) or metaluminous (Merguechoum, Tanncherfi). The composition of the Zekkara intrusion is meta- to peraluminous (El Hadi et al., 2006). All the samples from this study show

isotropic texture at macro and microscopic scale. More details on the samples and lithologies can be found in Supplementary material 1.

3.2. Analytical Procedure and Material

U–Pb geochronological measurements on zircon from the Jebilet and High Moulouya massif were performed at the Czech Geological Survey, Prague, on an Analyte Excite 193 nm excimer laser-ablation system (LA; Photon Machines), equipped with a two-volume HelEx ablation cell, in tandem with an Agilent 7900x ICPMS (Agilent Technologies Inc., Santa Clara, USA). Samples were ablated in He atmosphere (0.8 l min-1), and the laser was operated at 8 Hz using a spot size of 25 μm and laser fluence of 7.59 J cm-2. Each measurement consisted of 20 s of blank acquisition followed by ablation of the sample for a further 40 s. Multiple analyses were collected in a single mass spectrometer file with runs of the 91500 reference zircon interspersed between each set of 15 unknowns. Data were collected for masses 202, 204, 206, 207, 208, 232 and 238 using the SEM detector, with one point per mass peak and respective dwell times of 10, 10, 15, 30, 20, 10 and 15 ms per mass (total sweep time of 0.134 s). Data deconvolution using Iolite© followed the method described by Paton et al. (2010), which involves subtraction of an 'on peak' gas blank followed by correction for laser-induced elemental fractionation (LIEF) by comparison with the behaviour of the 91500-reference zircon (Wiedenbeck et al., 1995). No common Pb correction was applied. Zircon reference samples GJ-1 (~609 Ma; Jackson et al., 2004) and Plešovice (338 ± 1 Ma; Sláma et al., 2008) analysed periodically during this study yielded concordia ages of 609.0 ± 1.7 Ma and 338.3 ± 1.1 Ma (2σ), respectively.

U–Pb geochronological measurements on zircon from the Horsts belt were done at the Géosciences Paris-Saclay (GEOPS) laboratory (Paris Saclay) using LA–HR–ICP–MS. It uses a High Resolution ICP–MS ELEMENT XR (Thermo-Fisher Scientific) coupled with a 193 nm ArF Photon Machines (Teledyne) laser. The laser beam diameter was set at 40 μm for standards

and samples. Ablation conditions are a fluence of 2.5 J.cm^{-2} and a frequency of 10 Hz. Glass standards (NIST612 and NIST610) were analysed simultaneously. Each analysis consists of 30 seconds background acquisition followed by 30 s of sample acquisition and 30 s of washout. The laser-induced aerosol was carried by helium (large volume at 0. 5 l.min^{-1} and inner cup at 0. 375 l.min-1) from the sample cell to a mixing funnel in which the sample and He are mixed with 0.950 to 1 l.min^{-1} argon to stabilize the aerosol input to the plasma. Signal strength of the ICP-MS was tuned for maximum sensitivity while keeping Th/U between 0.97 and 1.03 and ThO/Th below 0.3 on NIST612. Isotopes ^{202}Hg, ^{204}(Pb+Hg), ^{206}Pb, ^{207}Pb, ^{208}Pb, ^{232}Th and ^{238}U were acquired with integration time per peak (ms) of 10 ms by 70 runs for all isotopes except ^{207}Pb with 20 ms. Analyses were standardized with zircon 91500 (1065 Ma; Wiedenbeck et al., 1995) interspersed every 10 samples and controlled with the Plešovice standard (338 ± 1 Ma; Sláma et al., 2008) interspersed every 20 samples which yielded concordia ages of 338 ± 2 Ma (2σ). Data reduction was processed using Iolite©. No common Pb correction was applied.

U–Pb data can be found in Supplementary material 2, 3 and 4.

3.3. Data processing

The analytical data has been processed using the IsoplotR toolbox (Vermeesch, 2018). Data reduction follows the recommendation of Spencer *et al.* (2016) whereby data is treated as concordant if the 2-σ ellipse overlaps with the concordia, and the preferred ages are single zircon concordia ages following the recommendations of Nemchin and Cawood (2005) and Zimmermann *et al.* (2018). We kept U–Pb zircon ages with a concordance level of 97–103% (defined as [^{206}Pb/^{238}U age]/[^{207}Pb/^{235}U age]*100 or as [^{207}Pb/^{206}Pb age]/[^{207}Pb/^{235}U age]*100 for ages older than 1200 Ma).

3. Results

3.2.1. Jebilet massif

Zircons from the Oulad Ouaslam granodiorite (J13A) in the Jebilet massif are elongated, mostly prismatic to sub-rounded grains (generally 100–400 μm in length) with a well-developed oscillatory zoning (Fig. 3). From the 171 spots realized on 101 zircons, 111 of the obtained data are concordant and show a spread from 370 to 318 Ma. A single concordant outlier gives an age of ca. 730 Ma. Based on spot locations, three main populations can be deciphered at ca. 346 Ma (n = 13), ca. 335 Ma (n = 63) mainly from zircon cores and ca. 322 Ma (n = 25) generally obtained from zircon rims (Fig. 3). The zircon grains from the main population (ca. 335 Ma) are generally small (~50–300 μm in length), darker and exhibit a well-developed prismatic shape. The longest and larger (up to 500 μm in length) zircon grains show generally cores at ca. 335 Ma and rims at ca. 322 Ma. All zircon grains from these populations have U contents mainly < 500 ppm. The Th/U ratio in zircon are generally < 1 (only a single outlier at 1.09, Fig. 3) and show similar variations between populations (0.17–0.9, Fig. 3).

3.2.2. High Moulouya massif

El Hassir granodiorite (M13A)

Zircons grains from the El Hassir granodiorite (M13A) are mostly prismatic to sub-rounded (generally 100–200 μm in length). Under CL, most of the grains exhibit concentric oscillatory zoning characteristic of igneous zircon. Few grains show CL-grey to dark zircon cores often overgrown by oscillatory zoning domains. Some grains show oscillatory zoning internal texture partially replaced by CL-bright patterns (Fig. 4a). A total of 91 concordant analyses from the 107 spots on 66 grains were measured for sample M13A and display a continuous array of ages between 318 and 388 Ma with a single outlier at ca. 580 Ma (Fig. 4a). A weighted mean age of 343.1 ± 1.2 Ma (MSWD = 0.82, n = 19) or an intercept age of 342.8 ± 1.6 Ma (MSWD = 0.95) can be calculated from CL-grey to dark zircon cores (Fig. 4a). Oscillatory zoned domain

analyses define a cluster (Fig. 4a) with a weighted mean age of 329.7 ± 0.8 Ma (MSWD = 0.78, n = 45) or an intercept age of 328.9 ± 1.1 Ma (MSWD = 0.86). Analyses from CL-bright zircon grains give a weighted mean age of 321.1 ± 1.3 Ma (MSWD = 0.19, n = 17) or an intercept age of 320.1 ± 1.7 Ma (MSWD = 0.21). All zircon grains have U contents mainly < 430 ppm. The Th/U ratio in zircon are generally < 1 (0.6 – 0.9) and show similar to slightly higher mean values (Fig. 4a) between the populations at 343 Ma (mean = 0.69), 330 Ma (mean = 0.75) and 320 Ma (mean = 0.8).

Calc-alkaline "grey" granite (M14)

Zircon grains from the Calc-alkaline "grey" granite (M14) are similar to those of El Hassir granodiorite (M13A). Most of the grains are prismatic (generally 50–150 μm in length) and show clear CL-dark to grey oscillatory zoned cores which are sometimes overgrown by homogeneous CL-dark to grey rims (Fig. 4b). Only 35 of a total of 98 analyses on 58 grains produced concordant ages. Most of the concordant data from oscillatory zoned cores show a spread of ages from 390 to 330 Ma. Two older concordant ellipses are noted at ca. 460–470 Ma and a single one at ca. 630 Ma (Fig. 4b). Concordant zircon analyses obtained from CL-dark oscillatory zoned cores give a weighted mean age of 353.1 ± 3.2 Ma (MSWD = 0.40, n = 6) or an intercept age of 342.8 ± 12 Ma (MSWD = 0.75). Analyses from CL-grey oscillatory zoned domains yield a younger weighted mean age of 337.0 ± 1.6 Ma (MSWD = 1.08, n = 15) or an intercept age of 328.9 ± 7.4 Ma (MSWD = 0.30). The homogeneous CL-grey to dark rim analyses define a cluster with a weighted mean age of 327.1 ± 2.4 Ma (MSWD = 0.37, n = 8) or an intercept age of 322.1 ± 10 Ma (MSWD = 0.36). All zircon grains have U contents mainly < 600 ppm. The older core population (ca. 353–343 Ma) shows consistent Th/U ratios (0.56–0.74; mean value = 0.65) while the large population at ca. 337–329 Ma exhibits significant variations between 0.16 and 1.15 (Fig. 4b). The younger rim population (ca. 327–322 Ma) shows less variations than the large population (Th/U = 0.4–0.86; mean value = 0.64).

Perdreaux two-mica granite (M11)

Zircons from the Perdreaux two-mica granite (M11) are mostly prismatic grains (generally 50–100 μm in length) and show well-developed oscillatory zoning. CL-grey internal textures that are overgrown by homogeneous CL-dark rims are observed for few grains (Fig. 4c). Sample M11 shows a high degree of discordance with only 20 concordant analyses from a total of 59 analyses on 38 grains. A small old population, obtained on homogeneous CL-grey cores (n = 3), give a poorly defined age at around 2000 Ma. Few core analyses (n = 6), characterized by mainly higher Th/U ratios (0.22 – 1.91), show a scattered range of concordant ages between 630 and 555 Ma (Fig. 4c). The main part of the dataset displays a restricted array of ages between 325 and 360 Ma. The well-developed oscillatory zoned zircon domains define a small cluster (Fig. 4c) with a weighted mean age of 339.6 ± 1.9 Ma (MSWD = 1.04, n = 4) or an intercept age of 337.8 ± 4.4 Ma (MSWD = 3.2). A weighted mean age of 326.8 ± 1.6 Ma (MSWD = 0.86, n = 5) or an intercept age of 319.6 ± 4.4 Ma (MSWD = 3.7) can be calculated from homogeneous CL-dark rims. All zircon grains have U contents mainly < 700 ppm. The Th/U ratio in zircon are generally < 1 and show similar variations between populations (0.17–0.54, Fig. 4c).

3.2.3. Horsts belt and Beni Snassen massif

Beni Snassen (J6-1)

Zircons from the monzogranite of Beni Snassen massif are mostly prismatic grains (> 200 μm in length) and exhibit concentric oscillatory zoning (Fig. 5a). From the 31 analyses realized on 31 grains, 16 of the obtained data are concordant and show a limited spread from 330 to 290 Ma. Three core analyses obtained on smaller and CL-dark zircon grains characterized by higher U contents (~600 ppm), give a poorly defined age at around 320 Ma (Fig. 5a). Based on spot locations, two populations can be deciphered at ca. 308 Ma (n = 9) for oscillatory zoned cores and at ca. 290 Ma (n = 4) generally obtained from zircon rims (Fig. 5a). All zircon grains have

U contents mainly < 600 ppm. The Th/U ratios in zircon are generally < 1 and show similar variations between populations (0.31–0.84).

Merguechoum massif (J5-2)

Zircons from the enclave-bearing amphibole granite of Merguechoum massif are prismatic to sub-rounded grains (100–300 µm in length) with oscillatory cores (Fig. 5b). Only 12 concordant analyses from the 24 were measured for sample J5-2. The main part of the dataset displays a restricted array of ages between 330 and 365 Ma (Fig. 5b) and yield a weighted mean age of 345.24 ± 2.8 Ma (MSWD = 0.68, n = 10) or an intercept age of 343.8 ± 4 Ma (MSWD = 1.1). All zircon grains have high U contents mainly between 500 and 700 ppm and high Th/U ratios (0.60–1.14).

Boudoufoud massf (J5-1)

Zircon grains from the biotite-granite of Boudoufoud massif show an elongated prismatic shape (often > 300 µm in length). Some grains show clear CL-dark to grey oscillatory zoned patterns (Fig. 5c). Only a few grains are sub-rounded. A total of 38 concordant analyses from the 49 spots on 49 grains were measured and display a continuous array of ages between 280 and 320 Ma with a younger outlier at ca. 230 Ma and an older one at ca. 345 (Fig. 5c). Four analyses, obtained on homogeneous zircons cores, give a poorly defined age at around 320 Ma (Fig. 5c). Concordant zircon analyses obtained from CL-dark oscillatory zoned domains define a weighted mean age of 305.2 ± 1.4 Ma (MSWD = 0.37, n = 14) or an intercept age of 306.1 ± 3.6 Ma (MSWD = 2.5). Analyses from CL-grey to bright or blurred oscillatory zoned domains yield a younger weighted mean age of 290.9 Ma ± 2.1 Ma (MSWD = 0.50, n = 17) or an intercept age of 291.3 ± 3.4 Ma (MSWD = 1.5). All zircon grains have high U contents mainly between 350 and 1100 ppm. The Th/U ratio in zircon are generally < 1 and show similar variations between populations (0.35–0.85).

Tanncherfi massif (J4-7)

Zircons from the biotite-granodiorite facies in the Tanncherfi massif are mostly prismatic grains (100–300 μm in length) and show clear oscillatory zoned patterns, sometimes overgrown by homogeneous CL-grey rims. Few grains show CL-grey or blurred oscillatory zoned internal texture (Fig. 5d). 32 concordant analyses were recorded from 49 total analyses on 49 zircon grains and show a spread of dates from 325 to 285 Ma (Fig. 5d). A weighted mean age of 317.1 ± 3.2 Ma (MSWD = 0.48, n = 7) or an intercept age of 316.1 ± 4.9 Ma (MSWD = 0.25) can be calculated from homogeneous CL-grey cores of small grains (~100 μm) (Fig. 5d). The oscillatory zoned domains define a cluster (Fig. 5d) with a weighted mean age of 303.5 ± 1.7 Ma (MSWD = 0.87, n = 19) or an intercept age of 303.3 ± 3.4 Ma (MSWD = 0.74). Analyses from CL-grey or blurred oscillatory zoned domains yield a younger weighted mean age of 292.4 ± 3.7 Ma (MSWD = 0.58, n = 7) or an intercept age of 287.1 ± 6.2 Ma (MSWD = 0.53). All zircon grains from these populations have quite low U contents mainly < 380 ppm. The Th/U ratio in zircon are high (0.66–1.35, mean value = 0.93) and show similar variations between populations (Fig. 5d).

Zekkara massif (J4-1)

Zircons from the amphibole-bearing granodiorite of the Zekkara massif are small prismatic to sub-rounded grains (< 200 μm in length) and show a well-developed oscillatory zoning under CL (Fig. 5e). Thirty-three of a total of 42 analyses on 42 grains produced concordant ages and display a continuous array of dates between 330 and 365 Ma. A single concordant outlier gives a slightly older age of ca. 400 Ma and another one yields a Paleoproterozoic age (ca. 1845 Ma, Fig. 5e). The main part of the dataset gives a weighted mean age of 348.0 ± 2.3 Ma (MSWD = 1.18; n = 27) or an intercept age of 342.8 ± 12 Ma (MSWD = 0.75). All zircon grains have U contents < 450 ppm and high Th/U ratios (0.65–1.21, mean value = 0.84).

4. Discussion

We first interpret the acquired U–Pb ages and discuss the significance of individual zircon populations. Subsequently regional tectonic implications of Meseta granitoid ages are discussed in terms of two major pulses. Finally, the magmatic activity and associated tectonic events of the Moroccan Meseta are compared to that in the European Variscan belt and some possible relations are discussed.

4.1. Interpretation of the U–Pb ages

4.1.1. Jebilet massif

Delchini et al. (2018) dated 4 samples (LA–ICP–MS on zircon) from different outcrops of the same intrusion which gave ages of 337 ± 4 (MSWD = 0.94, n = 24), 344 ± 3 (MSWD = 0.32, n = 15), 343 ± 7 (MSWD = 0.90, n = 19), and 348 ± 8 Ma (MSWD = 0.51, n = 12). They also obtained similar ages (LA–ICP–MS on zircon) from the nearby smaller Tabouchent-Bamega granodiorite intrusions (336 ± 4 Ma; 337± 4 Ma; 346 ± 10 Ma; 358 ± 7 Ma) and the westward Koudiat Hamra felsic intrusion (345 ± 2 Ma), i.e. older than the Koudiat Bouzlaf microgranite dated at $330.5^{+0,68}_{-0,83}$ Ma (U–Pb ID–TIMS on zircon) by Essaifi et al. (2003). Delchini et al. (2018) interpreted the ages as reflecting crystallization ages related to granitoid emplacement whereas some younger analyses were interpreted as a result of late Pb loss. However, Delchini et al. (2018) question the validity of the oldest age at ca. 358 Ma (i.e at the Devonian-Carboniferous limit) due to the dispersion of the analytical points. The existence of a Famenian–Tournaisian effusive activity was proposed by Kharbouch (1994) further North in the Sidi Bettache basin (Fig. 1), but without robust chronostratigraphic ages. In our study, the analyses of different CL domains of single zircon grains (core versus rim, dark versus bright) permit to define more precisely the magmatic activity related to the Oulad Ouaslam pluton emplacement. In sample J13A, the oldest age population at ca. 346 Ma (n = 13) obtained on CL-grey zircon cores (Fig. 3), may correspond to the onset of partial melting of deeper crustal source. The peak of magmatic activity is shown by the main population characterized by clear oscillatory zoned

domains dated at ca. 335.2 ± 0.8 Ma (n = 60) whereas the younger population of ages at ca. 323 Ma (n = 26), mostly calculated from zircon rims (Fig. 3), could reflect late to post-magmatic zircon crystallization. Based on a geochemical and Sr–Nd isotopic study, Essaifi et al. (2014) proposed that the felsic intrusions in the Jebilet massif originated from the partial melting of pelitic sediments due to mafic injection. The T_{DM} model ages (1.76–0.85 Ga) from the same study highlight a Proterozoic source. It is compatible with a single grain concordant age at 735 Ma (this study) or ca. 700 and 800 Ma inherited ages reported by Delchini et al. (2018). A similar age at ca. 699 Ma from a zircon core was also obtained from one granitic xenolith in Triassic lamprophyre (Dostal et al., 2005). We can therefore postulate the presence of a Cryogenian (Neoproterozoic) basement in the Jebilet Massif. Indeed, in the Meseta, the occurrence of Precambrian basement has been documented in the Western High Atlas (Eddif et al., 2007; Ouanaimi et al., 2018; Berrada et al., 2022), in the Rehamna massif (Baudin et al., 2003; Pereira et al., 2015b), in the Central massif (Tahiri et al., 2010; Pereira et al., 2014; Ouabid et al., 2017, 2020; Letsch et al., 2018) and in the Coastal Block and offschore in the Mazagan escarpment (El Houicha et al., 2018; El Haibi et al., 2020; Kuiper et al., 2021).

4.1.2. High Moulouya massif

The main U–Pb age populations obtained from oscillatory zoned cores define a very short time interval defined by ages at 339.6 ± 1.9 Ma (n = 5) for the Perdreaux granite (M11), 337.0 ± 1.6 (n = 15) Ma for calc-alkaline “grey” granite (M14), and 329.7 ± 0.8 Ma (n = 45) for El Hassir granodiorite (M13A) (Fig. 4). These new ages contrast with the younger ages obtained for the grey granite (ca. 319 Ma) and Perdreaux granite (ca. 281 Ma) measured from previous studies (Rb-Sr, Clauer, 1980; U–Pb zircon, ID-TIMS, Oukemeni et al., 1995). Only the age of the El Hassir granodiorite overlaps within uncertainty at 2σ the age of 333 ± 2 Ma (U–Pb zircon, ID-TIMS) obtained by Oukemeni et al. (1995). We suggest that the pink granite should have a

similar age because previous petrological studies demonstrated the cogenesis of the pink and grey granites (Oukemeni & Bourne, 1993).

Our data indicates that the magmatic activity at the High Moulouya massif was not long-lived, as proposed in previous multiple injection model (Oukemeni et al., 1995) but restricted to the late Visean interval. However, the thermal activity and partial melting of deeper crustal source may have started before, as shown by the oldest age populations found in the El Hassir granodiorite and grey granite as indicated by 343 ± 1 (n = 19) and 353 ± 3 Ma (n = 6) age populations. The younger populations (ca. 321–327 Ma) obtained on CL-bright zircon grains or on zircon rims in both the Perdreaux granite (M11) and the El Hassir granitoid (M13A) could reflect either late to post magmatic recrystallization or post-crystallization disturbance by late fluid activity leading to U loss (Schaltegger et al. 1999; Corfu et al. 2003 and reference therein). Structural data agree with a syntectonic emplacement within a sub-horizontal ductile shear zone (Diot & Bouchez, 1989; 1991; El Mouraouah, et al., 1993). This main sub-horizontal metamorphic foliation from the High Moulouya massif is interpreted to reflect the Eovariscan event described in the Meseta (Hoepffner, 1987). Therefore, our data permit to refine the timing of this event to the Visean, or even down to the Tournaisian if we consider the oldest zircon 353 Ma population, even though the tectonic signification of this event, i.e. compressional (Allary et al., 1976; Hoepffner, 1987; Bouabdelli, 1989; Lahfid et al., 2019; Accotto et al., 2020) or extensional (Diot & Bouchez, 1989; El Mouraouah et al., 1993; Houari, 2003; Leprêtre et al., 2020), is still debated.

We underline the magmatic activity in the High Moulouya was associated with the formation of late Visean intracontinental basins in the Eastern Meseta (Berkhili et al., 1993), similar to what have been observed in the Jebilet massif. On the basis of the synchronicity between formation of (mid-) late Visean sedimentary basins and age of studied syntectonic granitoids (ca. 340–330 Ma) we can postulate that the metamorphic sub-horizontal foliation

and localized recumbent folds observed in the High Moulouya massif could be compatible with a general extension as already suggested by Diot and Bouchez (1989). The beginning of HT event can be deduced from the petrological study of Elabouyi et al. (2019). These authors attributed the chemistry of garnet core and biotite, sillimanite and quartz inclusions in the garnet preserved in the anatectic granite to the partial melting event preceding the final emplacement and crystallization of the granitoids. The onset of this HT event was probably dated by the oldest zircon populations (ca. 343–353 Ma) from this study implying that the extension has started already in the Tournaisian and culminated at the mid-late Visean. The progressive crustal stretching probably enhanced the partial melting of the subcontinental mantle and the crust leading to the production of the High Moulouya granitoid complex. Late injection of pegmatite veins might be responsible for the rejuvenation of some zircons at ca. 321–327 Ma. U–Pb data on zircon from the pegmatite, microgranite or aplite dykes are not available, but it is likely that Rb–Sr ages from Clauer et al. (1980) at ca. 300–310 Ma underestimate the final age of the magmatic activity in the region.

The presence of a Precambrian basement below the High Moulouya massif has been proposed by Oukemeni et al. (1995) based on U–Pb zircon discordia at 1520 Ma for the granodiorite and 1245 and 1804 Ma for the grey granite. Inherited zircons from this study provide further information about the nature of the basement. Several analysed samples are supplemented by a few Paleoproterozoic (1960–2025 Ma, sample M11, Perdreaux granite) and Neoproterozoic ages (550–650 Ma, samples M11 and M13A). Previous geochronological and geochemical studies proposed different sources for the magmatism in the High Moulouya massif (Oukemeni & Bourne, 1993; Gasquet et al., 1996; Elabouyi et a., 2019). The later suggested that the per-aluminous S-Type Perdreaux granite resulted from the anatexis of a Proterozoic middle crustal metapelite protolith. This agrees with the presence of inherited Proterozoic zircons which may correspond to detrital zircon grains in the sedimentary source.

The 550 Ma inherited zircons could indicate the maximum depositional age of metapelite. The Neo and Paleoproterozoic zircon populations are well known in the sediments of the north Gondwana margin and reflect the sedimentary recycling of the Eburnean and Pan-African orogenies (e.g. Ghienne et al., 2018).

In contrary, a more juvenile source has been proposed for the El Hassir granodiorite based on Lu–Hf in zircon isotopic data (El Mouraouah, 1994). As proposed by Elabouyi et al. (2019), the intrusion of juvenile and mafic magmas in the middle crust could have triggered its partial melting and the formation of felsic S-type magmas. In this model, the El Hassir granodiorite represents the less evolved juvenile magma whereas the grey and pink granites represent more fractionated felsic magmas. Nevertheless, the presence of Neoproterozoic inherited zircons (both in the El Hassir granodiorite and grey granite) may indicate a crustal contamination/assimilation or a mixed crustal and mantle origin as proposed for the grey granite based on Sr isotopes (Mrini et al., 1992).

4.1.3. Horsts belt

Apart from the Tanncherfi massif, all determined ages are older than the previously published data, by ca. 50 to 15 Ma. The new U–Pb ages (Fig. 5) measured in granitoids of the Horsts belt are ranging from 350 to 290 Ma, compared to the ca. 330–250 Ma range obtained by the Rb–Sr method (Mrini et al., 1992; Ajaji et al., 1998). From our data, we distinguished one group of early Carboniferous ages (ca. 350–340 Ma) and another one of late Carboniferous ages (ca. 310–300 Ma).

In the first group, two samples, one from Zekkara (J4-1) and another one from the Merguechoum (J5-2) massifs provide main populations from oscillatory zoned cores at 348.1 ± 2.3 Ma (n = 27) and 345.2 ± 2.8 Ma (n = 10), respectively (Fig. 5 e,b). We interpret these ages to reflect the first main early Carboniferous magmatic episode. Indeed, those late Tournaisian – early Visean ages are slightly older than the mid to late Visean volcanic activity

in the area, as shown by the intermediate to felsic lavas intercalated with Visean sediments in the Horsts belt (e.g. in the Tanncherfi massif) or in the nearby Jerada basin (Kharbouch, 1982, 1994). The Rb–Sr ages from whole-rock isochrones obtained at 287 ± 8 Ma (i.e. early Permian) and 321 ± 15 Ma by Mrini et al. (1992) for the Zekkara and Merguechoum intrusions, respectively, cannot thus correspond to intrusion or crystallization ages. Only one inherited zircon of Paleoproterozoic age dated at ca. 1846 Ma reflects detrital zircon ages typically found in sediments derived from the West African Craton.

The next younger group of samples provided populations of late Carboniferous – early Permian ages. In Tanncherfi, an age of 303.5 ± 1.7 Ma (n = 19) was obtained on oscillatory zoned zircons from the biotite-granodiorite (J4-7) and is interpreted as the emplacement age (Fig. 5d). The Tanncherfi massif was previously dated at 286 Ma ± 10 Ma by Mrini et al. (1992) using Rb–Sr isochrones on several facies (monzogranite, monzodiorite, granodiorite and aplite). In contrary, Ajaji et al. (1998) divided the magmatic complex into two series: a K series and a Na series which includes the granodiorite sample from this study. They obtained for the K series an age of 344 ± 6 Ma (Rb–Sr whole-rock isochron) whereas the younger age of 325 ± 10 Ma for the Na series was discarded because of its high MSWD (3.89). Therefore, in the light of our new result, we can speculate that the Na series mainly emplaced at ca. 303 Ma, i.e. at the end of the Carboniferous and that the K series could be as old as Visean (344 ± 6 Ma, Rb-Sr whole rock isochron) as shown by Ajaji et al. (1998).

In the Boudoufoud massif, the age of 305.2 ± 1.4 Ma (n = 14) obtained on oscillatory zircons is interpreted as reflecting the emplacement age of the magmatic complex (Fig. 5c). This Late Carboniferous age is much older compared to ages obtained by Tisserant (1977) at 266 ± 9 Ma or by Mrini et al. (1992) at 259 ± 11 Ma with the Rb–Sr whole-rock isochron. The second zircon age population gives an age of 290.9 ± 2.1 Ma (n = 17) which may be also related to late to post magmatic recrystallization or late fluid circulation possibly responsible for the

rejuvenation of Rb–Sr ages. Finally, the four oldest concordant analyses of zircon cores defining an age of 318 Ma might correspond to the age of the onset of anatexis preceding granite crystallization.

In the Beni Snassen granite, the main age population at 308.2 ± 2.7 Ma (n = 9) obtained from oscillatory zoned zircon crystals probably reflects the main magmatic event (Fig. 5a). The older age population at 323.4 ± 6.9 Ma (n = 3) obtained on small and dark luminescent zircon grains may represent crystals that grew during the early stage of crustal anatexis, similarly to the Boudoufoud magmatic complex. Therefore, based on our new data, the magmatism in the Beni Snassen massif is late Carboniferous and not early Triassic as previously suggested by a Rb–Sr whole-rock isochron (Mrini et al., 1992).

4.2. Regional implications

The last compilations by El Hadi et al. (2003, 2006), defined four magmatic pulses at ca. 330, 320–300, 290–270 and 270–260 Ma mostly based on Rb-Sr ages from the literature. Available U–Pb data obtained on zircon crystals from this study and from published data indicated that these periods of magmatism should be re-evaluated. In the following, based on our new results and some published robust geochronological data, two different magmatic episodes with contrasted geodynamic significance are proposed.

4.2.1. Late Devonian – Visean magmatic episode

Our data highlight a magmatic episode restricted to the Tournaisian – Visean interval in the Jebilet and High Moulouya massifs and in the Horsts belt (Zekkara, Merguechoum)(Fig. 6). Similar ages of intrusions where already reported for the potasic magmatic series in the Tanncherfi massif (Rb-Sr, Ajaji et al. [1998]), the Lalla Tittaf rhyolite in the Rehamna massif (U–Pb zircon age, Aït Lahna et al., 2018), and intrusive rocks (U–Pb zircon ages, Essaifi et al. [2003], Delchini et al. [2018] and Aït Lahna et al. [2018]) and rhyolitic lavas ($^{40}Ar/^{39}Ar$ on sericite, Marcoux et al. [2005]) from the Jebilet massif (Fig. 6). Similar ages were also proposed

but without isotopic dating for intrusions in the Tazekka (Huvelin, 1992), the Mekkam (Huvelin, 1983) or Merguechoum massifs (Muratet, 1994). Our new results indicate that the main pulse of this first magmatic period occurred between 350 and 330 Ma at the scale of the whole Meseta (Figs. 6, 7, 8), contributing to the early heating of the Carboniferous basins and their basement as shown by the widespread HT–LP metamorphism in early Carboniferous basins in the Jebilet massif (Dostal et al., 2005; Delchini et al., 2016), or by the presence of early andalusite porphyroblasts in the Lalla Tittaf schists in the Rehamna massif (Wernert et al., 2016) and in xenoliths' metasedimentary protoliths from the Moroccan Massif Central in the area of Mrirt (Duchêne et al., 2022). Obviously, this does not preclude the possibility that this magmatic pulse may have started earlier in some part of the belt, since slightly older zircons in Jebilet, High Moulouya, Zekkara and Merguechoum massifs are measured with late Devonian to Tournaisian concordant ages. The partial melting of crustal source preceding the main intrusive phase may be triggered by the emplacement of mafic magmatic rocks in the deep crust as reflected by mafic enclaves in slightly younger granitoids (Essaifi et al., 2014). Together with our new datings from Jebilet massif, other U–Pb ages suggested the possible late Devonian – Tournaisian contribution to the earliest magmatic activity also in Western Meseta (Delchini et al., 2018). Importantly, this magmatic episode ended at around 330 Ma (Figs. 6, 7).

The geodynamic context explaining this early magmatic activity is still debated (Hoepffner et al., 2005). Although we suggest a major episode of magmatism during Visean, earlier studies envisaged that the Eovariscan deformation phase was associated with a volcanic arc activity restricted to the Eastern Meseta. Piqué & Michard (1989) then Michard et al. (2010) emphasize the occurrence of unconformable, arc-type Upper Visean andesitic-felsic lava flows on top of the folded Ordovician-Devonian series of Eastern Meseta, in a supra-subduction setting. Accotto et al. (2020) consider the hypothesis of an Avalonian arc that would have

impinged the Eastern Meseta crust and then retreated. The senses of subduction are opposite, south-eastward for Michard et al. (2010), north-westward for Accotto et al. (2020). However, the presence of a major magmatic centre in the Jebilet indicates that the magmatism affected the whole Meseta domain. Furthermore, the witnesses of a subduction zone in the Meseta (either of the Rheic or Paleothetys ocean) is mainly based on the presence of early Carboniferous arc-like volcanism (Kharbouch et al., 1985, Kharbouch, 1994). However, this chemical signature could reflect the inherited metasomatized nature of the mantle source (Chalot-Prat, 1995; Driouch et al. 2010; Ajaji et al. 1998) or crustal contamination (e.g. Xia and Li, 2019). We argue that the geodynamic context of the formation of the basins in the Meseta could be an intracontinental context not implying back-arc extension. In this context, the Eovariscan schistosity, HT-LP metamorphism and associated sub-horizontal shearing in the Meseta could be formed during an extensional phase at the north-western edge of Gondwana since the Upper Devonian (Frizon de Lamotte et al., 2013). Finally, this extension could culminate with the intrusion of granitoids at ca. 350–330 Ma in the whole Meseta (Fig. 7, 8).

4.2.2. Late Carboniferous-Cisuralian magmatic episode

Our data agree with a second magmatic stage restricted to the very late Carboniferous – Cisuralian: 303.5 ± 1.7 Ma at Tanncherfi, 305.2 ± 1.4 Ma at Boudoufoud and 308.2 ± 2.7 Ma at Beni Snassen (Fig. 6). An additional age for the Eastern Meseta is found in the Tiffrit/Saïda inlier (Algeria) at 297 ± 1 Ma (U–Pb on zircon; Remaci-Benaouda, 2005). Other similar ages are known in the Western Meseta in the 305–275 Ma period: e.g. 276 ± 3, 279 ± 2 and 295 ± 3 Ma for the Azegour, Bouzouga and Tawrirt granites in the Western High Atlas (U–Pb, Ettachfini et al., 2018; Fekkak et al., 2018); 285.2 ± 5.5 for the Ras el Abiod granite in the Rehamna massif ($^{40}Ar/^{39}Ar$ cooling ages, Chopin et al., 2014) or 284 ± 5 to 285 ± 6 Ma for andesites-rhyolites of the Mechra Ben Abbou Basin (U–Pb SHRIMP, Domeier et al., 2021); ca. 280–300 Ma in metasedimentary xenolith from the Jebilet massif (U–Pb SHRIMP on zircon,

Dostal et al., 2005) or 291 $^{+16}/_{-7}$ Ma for the Zaër (U–Pb TIMS on zircon, Cailleux et al., 2001) and 297 $^{+16}/_{-7}$ Ma for the Oulmès (U–Pb TIMS on zircon, Baudin et al., 2001) intrusions in the Moroccan Central Massif (Fig. 6). Studies by Marcoux et al. (2015) or Domeier et al. (2021) also showed the importance of volcanism in the easternmost Massif Central, with new U–Pb datings on zircon, ranging from 305 to 277 Ma. Some late/post-orogenic intrusions could be considered as a last magmatic pulse, e.g. at ca. 276 Ma for the Sebt Brikiine granite intrusion in the Rehamna ($^{40}Ar/^{39}Ar$ on biotite, Chopin et al., 2014). As a whole, this second magmatic period is thus consistently synchronous with the main late Carboniferous – Cisuralian contractional events (Chopin et al, 2014) affecting both Meseta. Indeed, similar ages have been obtained from metamorphic rocks in the Rehamna (from 310 to 280 Ma, $^{40}Ar/^{39}Ar$ on micas, Chopin et al. [2014]; ca. 298 & 276 Ma, U–Pb on monazites in Wernert et al. [2016]) or Jebilet (306 ± 1 Ma,$^{40}Ar/^{39}Ar$ on sericite in Essaifi et al. [2021]) massifs. Those ages have been interpreted as resulting from the formation of the intracontinental variscan belt in the Meseta (Hoepffner et al., 2005) into two major convergent steps reflecting global reorganization during the formation of Pangea (Chopin et al., 2014; Wernert et al., 2016)(Fig. 7).

4.3. Comparison with the magmatic activity in the European Variscan belt

The tempos of magmatic activity in the European Variscan belt are contrasted to those of Northwest Africa (Figs. 7, 8). Syn-orogenic magmatism related to subduction and further collision is widespread in the Variscan Iberian massif at ca. 360–330 Ma (Figs. 7b, 8; see Martínez Catalán et al. 2021 for a review). It mainly consists of (1) per- to meta-aluminous biotite-rich granitoids derived from partial melting of the upper mantle and the thickened orogenic lower crust and (2) per-aluminous two-mica granitoids derived from partial melting of the middle crust. This syn-orogenic early Carboniferous magmatism was followed by a late Visean extensional event represented by the development of large extensional core complexes and main intrusive phase (Figs. 7b, 8) ranging from 325 to 310 Ma (Figs. 7b, 8; Martínez-

Catalán et al., 2014; Edel et al., 2018). Then, Gutiérrez-Alonso et al. (2011), proposed the following two-step evolution for late- to post-Variscan orogenic intrusions, which both give birth to first (hot) mafic and then (cold) felsic magmas. The first one at 310–300 Ma (Figs. 7b, 8) is supposed to be synchronous with the formation of the Cantabrian orocline (Gutiérrez-Alonso et al., 2004; Weil et al., 2012). It is associated with initial partial melting of the sub-continental lithosphere furtherly followed by progressive partial melting of the lower- to middle crust. The second one, at 300–285 Ma (Figs. 7b, 8), is interpreted as the consequence of the late orogenic delamination of the thickened lithosphere (Gutiérrez-Alonso et al. 2004; Fig. 7a). It results again in partial melting of the mantle and the orogenic crust due to asthenosphere upwelling, associated with minor extension and formation of post-orogenic basins (e.g. Ziegler and Dèzes, 2006). Alternatively, Pereira et al. (2015a) consider the ca. 315–280 Ma old calc-alkaline batholiths of the Iberia arc to be formed during the subduction of the Paleotethys oceanic plate.

A compilation of the magmatic evolution in the French Variscan Massif Central has been carried out by Rolin et al. (2009) and Vanderhaege et al. (2020). There, the first Upper Devonian tonalites and volcanites are interpreted as a supra-subduction arc type magmatism (Figs. 7a, 8; Pin and Paquette, 2002; Lardeaux et al., 2014). The early Carboniferous intrusive event was recognized and interpreted in terms of syncollisional magmatism where mantle- and crustal-derived magmatic rocks are formed in a thickened, mature orogenic plateau above a subducting plate (Vanderhaeghe et al., 2020). The subsequent magmatic event is associated with major NW-SE crustal extension crustal melting and activity of dextral and sinistral strike-slip faults and is bracketed between 330 and 310 Ma (Figs. 7a, 8, Faure et al., 2009, Rollin et al., 2009). It is associated with HT–LP metamorphism that affected mostly the western part of the French Massif Central (e.g. Faure et al., 2002, 2009 and references therein), interpreted in terms of syn-collisional extension or lateral spreading of the partially molten lower crust (Faure

et al., 2002). In the eastern French Massif Central, Laurent et al., (2017) and Vanderhaeghe et al., (2020) proposed a southward decrease of the age of granitoids from ca. 345 Ma to ca. 310 Ma which was interpreted in terms of a southward retreat of a northward subducting slab. The final magmatic stage (Figs. 7a, 8) was associated with the formation of the HT–LP migmatite Velay (Malavieille et al., 1990; Vanderhaeghe et al., 1999, Ledru et al., 2000; Gardien et al., 2022) and Montagne Noire dome (Poilvet et al., 2011; Poujol et al., 2017) during late Carboniferous – early Permian (300–295 Ma), both interpreted as a result of late orogenic gravitational collapse (Malavieille, 1993) of the partially molten orogenic root due to delamination of the oceanic slab.

However, for Franke et al. (2011), this late Carboniferous – early Permian HT event is not related to post-orogenic extension, but rather could be produced by a long-lasting plume system enhancing the westward propagation the Paleotethys ocean along a mega-shear zone within the European Variscan belt (e.g., Franke, 2014; Franke et al., 2017). The plume theory is based on spatial overlap of European Variscan belt with western margin of the Tuzo plume from ca 330 Ma, with maximum overlap of the Variscan belt with the central part of the plume at 290 Ma (Torsvik et al., 2014). Even if the plume theory was proposed already by Simancas et al., (2003, 2006) and Carbonell and Simancas (2004) based in 140 km long mid-crustal reflector in the IBERSEIS seismic profile, the geological evidences from Iberia are not convincing. Instead, most of authors consider Carboniferous gabbroic and basaltic magmatism to be linked to slab break-off following main phase of oceanic subduction (Pin et al., 2008) while Carboniferous HT event in Iberia and French Massif Central is considered to reflect post-orogenic collapse (Martínez-Catalán et al., 2014 for review; Costa and Rey, 1995; Faure et al., 2009).

4.4. Magmatic evolution in the variscan belt in a geodynamic context

Our results combined with a compilation of robust U–Pb or $^{40}Ar/^{39}Ar$ ages from the Meseta highlight two main magmatic events with contrasting tectonic settings compared to the European branch of the Variscan belt (Fig. 7c). The first one, early Carboniferous, group of magmas were emplaced at ca. 350–330 Ma (i.e. Tournaisian to Visean), i.e. synchronous with the formation of intracontinental, extensional basin in the whole Meseta. This magmatism forming both mafic mantle-derived magma (e.g. gabbro in the Jebilet and Rehamna massifs) and metaluminous granitoids (e.g. Oulad Ouaslam intrusion in the Jebilet, High Moulouya magmatic complex, or Zekkara and Merguechoum granitoids) operated synchronously with arc magmatism and further partial melting of the thickened orogenic root in Iberia and in the French Massif Central (e.g. Chelle-Michou et al., 2017; Fréville et al., 2022; Pereira et al., 2023) (Fig. 9a). We interpreted the early Carboniferous extensional event affecting Moroccan Meseta to be due to the fragmentation of Gondwana associated with the opening of the Paleotethys (Fig. 9a; Stampfli et al., 2003; 2013; Martínez-Catalán et al., 2021; Edel et al., 2018). Such a fragmentation may have started as soon as the Upper Devonian (Frizon de Lamotte et al., 2013). A similar bimodal association in Iberia (e.g. Beja magmatic complex, Jesus et al., 2007) have in contrary been interpreted as a magmatic activity in a suprasubduction setting, during the closure of either the Rheic or the Rhenohercynian ocean (see discussion in Martínez Catalán, 2021). Here, we propose that there can be a causal link between the two contrasting tectonic and magmatic Variscan provinces as shown in the simplified plate reconstructions in the Figure 9a (modified after Martínez Catalán et al., 2021): i.e. (1) propagation of the Paleotethys ocean's tip within the Meseta and (2) simultaneous closure of the Rheic ocean and further collision of Mid-Variscan allochthon (Avalonia) with the Mid-Variscan autochton (European variscan belt). However, the existence of the Paleotethys ocean before the Permian in this area is disputed (see Franke, 2014; Franke et al., 2017). Our model is also supported by detrital zircon studies

indicating major modification of detrital zircon spectra from Upper Devonian and early Carboniferous extensional basins, compatible with the erosion of orogenic topography further North (Jouhari et al., 2022). However, this modification is interpreted by Accotto et al. (2020) as reflecting the contractional, Eovariscan, southern propagation of the Avalonian promontory (Sehoul Block) towards the Meseta.

In contrast to early Carboniferous collision in the European Variscides, the (intracontinental) Variscan collisional event in the Meseta took place in two steps during late Carboniferous – early Permian (Fig. 9b and c; Chopin et al., 2014). The few oldest syn-orogenic magmatic intrusions in the Meseta are late Carboniferous (ca. 305 Ma, this study) and are synchronous with the oldest age from metamorphic rocks from the Rehamna massif (310 Ma, $^{40}Ar/^{39}Ar$ ages in Chopin et al. [2014]). This first tectonometamorphic event is interpreted as reflecting the onset of the collision of Gondwana with the European Varisan belt. Indeed, at that time (Fig. 9b,c), magmatism developed (1) in Iberia during the formation of the cantabrian orocline (Gutiérrez-Alonso et al., 2011), (2) in the Massif central during syn-orogenic extension (Faure et al., 2002) (Fig. 7, Fig. 8b). Therefore, the synorogenic magmatism and generalized shortening of northern Gondwana (Meseta) coincides with syn-compressional deformation of Iberian orocline and extension in the French Massif Central (Fig. 9b). Therefore, we propose that the restrained late Carboniferous magmatic activity in the Meseta is contemporaneous with the closure of intracontinental basins at the north Gondwana margin and the Paleotethys Ocean further East (see also Pereira et al., 2015b). This event is then followed by an early Permian head-on collision between Gondwana and Laurussia (Fig. 9c)(Chopin et al., 2014, Edel et al., 2015, 2018). In the Meseta, it enhanced the formation of late/post orogenic magmatism whereas in the European Variscan belt, the magmatism result from major late/post orogenic extension, maybe enhanced by a continuous retreat of northward subducting Paleotethys plate (Fig. 9c;

Gutiérrez-Alonso et al., 2008, Pereira et al., 2014; Laurent et al., 2017, Vanderhaeghe et al., 2020).

5. Conclusion

- New LA-ICP-MS U–Pb zircon data of intrusive rocks show the existence of two distinct early Carboniferous and late Carboniferous – early Permian magmatic pulses in the whole Meseta domain, and not three, as advocated in previous papers.
- Our new data outline for the first time a widespread intrusive, early Carboniferous (348-337 Ma) magmatic event in the Eastern Meseta.
- The first pulse of magmatism in the Meseta at ca. 350–330 Ma is synchronous with the Eovariscan phase and the development of intracontinental (?) basins in all the Meseta. We propose that it might be related to a generalized extension of the north Gondwana margin associated with the propagation of the Paleotethys ocean.
- After a gap of ca. 25–30 Myr, the second pulse of magmatism at 305–275 Ma is synchronous with the main variscan convergent event(s) in the Meseta, in a context of intracontinental orogeny. It is interpreted to result from collision of Gondwana with the Europena Variscan belt (closure of the Paleotethys Ocean propagator tip) followed by head-on collision with Laurussia.
- The two events are compared to magmatic events in main European Variscan branch, which leads to an updated tectonic model of Pangea formation.
- Our data are giving new clues on the age and nature of the basement bellow the Paleozoic cover.

Acknowledgement

This work was supported by the TelluS Program of CNRS/INSU and institutional grants from the Czech Geological Survey (grant number 310270 and DRKVO) and the CNRS UMR 7516

(IPGS). Jean-François Ghienne (Institut Terre & Environnement de Strasbourg UMR 7063) and José Ramón Martínez Catalán (Universidad de Salamanca) are thanked for helpful discussions together with the University Chouaib Doukkali for its support during the field work. We thank the reviewers André Michard, Wolfgang Franke and Antonio Castro for their corrections and comments. The authors acknowledge M. Santosh and Taras Gerya from the editorial board of Gondwana Research.

References

Accotto, C., Martínez Poyatos, D., Azor, A., Jabaloy-Sánchez, A., Talavera, C., Evans, N.J., Azdimousa, A., 2020. Tectonic Evolution of the Eastern Moroccan Meseta: From Late Devonian Forearc Sedimentation to Early Carboniferous Collision of an Avalonian Promontory. Tectonics 39, 1–29. https://doi.org/10.1029/2019TC005976

Accotto C., Martínez Poyatos D., Azor A., Talavera, C., Evans, N.J., Jabaloy-Sánchez, A., Azdimousa, A., Tahiri, A., El Hadi, H., 2021. Syn-collisional detrital zircon source evolution in the norther Moroccan Variscides. Gondwana Research 93, 73–88. https://dx.doi.org/10.1016/j.gr.2021.02.001

Aït Lahna, A., Aarab, E.M., Nasrrddine, Y., Colombo Celso Gaeata, T., Bensalah, M., Boumehdi, M.A., Kei, S., Basei, M.A.S., 2018. The Lalla Tittaf Formation (Rehamna, Morocco): Paleoproterozoic or Paleozoic age?, in: ICG2018-Joint Congress-CAAWG9-CAAWG9-ArabGU2-ICGAME3, Abstract Book, El Jadida, 13–16.

Ajaji, T., Weis, D., Giret, A., Bouabdellah, M., 1998. Coeval potassic and sodic calc-alkaline series in the post-collisional Hercynian Tanncherfi intrusive complex, northeastern Morocco: Geochemical, isotopic and geochronological evidence. Lithos 45, 371–393. https://doi.org/10.1016/S0024-4937(98)00040-1

Allary, A., Lavenu, A., Ribeyrolles, M., 1976. Étude tectonique et microtectonique d'un segment de chaîne hercynienne dans la partie sud-orientale du Maroc central. Notes et Mémoires du Service Géologique du Maroc 261, 169.

Amenzou, M., Aghchmi, E.M., Ouazzani, H., El Mouraouah, A.E.A, 2001. Signification géodynamique de la répartition spatiale des granitoïdes hercyniens du Maroc nord-oriental d'après la typologie des zircons. Notes et Mémoires du Service Géologique du Maroc 408, 37–48.

Andries, D., Benjamin, D., 1994. Carte géologique du Maroc au 1/50 000 – Feuille de Beni-Oukil, Notes et Mémoires du Service Géologique du Maroc 362.

Aretz, M., 2010. Rugose corals from the upper Viséan (Carboniferous) of the Jerada Massif (NE Morocco): Taxonomy, biostratigraphy, facies and palaeobiogeography. Palaontologische Zeitschrift 84, 323–344. https://doi.org/10.1007/s12542-009-0046-0

Baudin, T., Chevremont, P., Thieblemont, D., Rachdi, H., Roger, J., Razin, P., Benhaourch, R., Winckel, A., 2001. Notice explicative de la carte géologique du Maroc au 1/50 000 – Feuille d'Oulmès, Notes et Mémoires du Service Géologique du Maroc 410 bis.

Baudin, T., Chévremont, P., Razin, P., Youbi, N., Andries, D., Hoepffner, C., Thiéblemont, D., Chihani, E., Tegyey, M., 2003. Carte géologique du Maroc au 1/50 000 – Feuille de Skhour des Rehamna, Mémoire explicatif. Notes et Mémoires du Service Géologique du Maroc 435 bis, 1–114.

Beauchamp, J., 1984. Le Carbonifère inférieur des Jebilet et de l'Atlas de Marrakech (Maroc); migration et comblement d'un bassin marin. Bulletin de la Société Géologique de France 26, 1025–1032. https://doi.org/10.2113/gssgfbull.s7-xxvi.6.1025

Becker, R.T., El Hassani, A., 2020. Devonian to Lower Carboniferous stratigraphy and facies of the Moroccan Meseta: implications for palaeogeography and structural Interpretation - a project outline. Frontiers in Science and Engineering 10(1), 9–25. https://doi.org/10.34874/IMIST.PRSM/fsejournal-v10i1.27132

Becker, R.T., El Hassani, A., Aboussalam, Z.S., 2021. Devonian to Lower Carboniferous stratigraphy and facies of the South-Western Moroccan Meseta: Implications for paleogeography and structural interpretation. Frontiers in Science and Engineering 10(2), 337pp.

Ben Abbou, M., 2001. Dynamique des bassins d'avant-pays carbonifères, signatures tectoniques, sédimentaires et magmatiques de l'évolution de la chaîne hercynienne du

Maroc central septentrional : implication sur le modèle géodynamique de la chaîne hercynienne. Université Cadi Ayyad, Marrakech, Thèse ès Sciences.

Ben Abbou, M., Soula, J.-C., Brusset, S., Roddaz, M., N'Tarmouchant, A., Driouch, Y., Christophoul, F., Bouadbelli, M., Majesté-Menjoulas, C., Béziat, D., Debat, P., Déramond, J., 2001. Contrôle tectonique de la sédimentation dans le système de bassins d'avant-pays de la Meseta marocaine. Comptes Rendus de l'Académie des sciences, Série IIA - Earth and Planetary Science 332, 703–709. https://doi.org/10.1016/S1251-8050(01)01590-7

Berkhli, M., Paicheler, J.C., Vachard, D., 1993. Données nouvelles sur la stratigraphie des terrains carbonifères de la Meseta orientale marocaine (boutonnières de Debdou, Mekkam et Jerada). Geologische Rundschau 82, 84–100. https://doi.org/10.1007/BF00563272

Berkhli, M., Vachard, D., Paicheler, J.C., Tahiri, A., 2000. Modèle sédimentaire et évolution géodynamique du Nord-Est de la Meseta occidentale marocaine au cours du Carbonifère inferieur. Comptes Rendus de l'Académie des sciences, Série IIA - Earth and Planetary Science 331, 251–256. https://doi.org/10.1016/S1251-8050(00)01417-8

Berrada, I., Fekkak, A., Pereira, M.F., Jouhari, A., Ouanaimi, H., Leprêtre, R., Ezzouhairi, H., Gasquet, D., El Attari, A., El Houicha, M., 2022. Geochronological evidence of Cambrian Series 2 calc-alkaline plutonism in the Paleozoic Western High Atlas (Moroccan Meseta). Journal of African Earth Sciences 194, 104611. https://doi.org/10.1016/J.JAFREARSCI.2022.104611

Bordonaro, M., Gaillet, J.-L., Michard, A., 1979. Le géosynclinal carbonifère sud-mésetien dans les Jebilet (Maroc) ; une corrélation avec la province pyriteuse du Sud de L'Espagne. Comptes Rendus de l'Académie des sciences, Paris, série D 288, 1371–1374.

Bougara, M., Steemans, P., Le Hérissé, A., Boulvain, F., 2017. Palynologie et environnements des sédiments du Dévonien de Saïda (Algérie nord occidentale). Carnets de Géologie, 17(10), 191–219. http://doi.org/10.4267/2042/64285

Boulin, J., Bouabdelli, M., El Houicha, M., 1988. Evolution paléogéographique et géodynamique de la chaîne Paléozoïque du Moyen-Maroc : un essai de modélisation (Palaeogeographic and geodynamic evolution of the middle Morocco Paleozoic belt: an attempt at modelization). Comptes Rendus de l'Académie des sciences, Série II 306, 1501–1506.

Bouloton, J., 1992. Mise en évidence de cordiérite héritée des terrains traversés dans le pluton granitique des Oulad Ouaslam (Jebilet, Maroc). Canadian Journal of Earth Sciences 29(4), 658–668. https://doi.org/10.1139/e92-057

Bouloton, J., Gasquet, D., 1995. Melting and undercooled crystallisation of felsic xenolithsfrom minor intrusions (Jebilet massif, Morocco). Lithos 35, 201–219.https://doi.org/10.1016/0024-4937(94)00051-3

Bouloton, J., El Amrani, I.E., El Mouraouah, A.A., Montel, J.-M., 1991. Les xénolites hyperalumineux des granites, d'après l'exemple du pluton superficiel des Oulad Ouaslam (Jebilet, Maroc). Comptes Rendus de l'Académie des sciences, Série II 312, 273–279.

Bouloton, J., Gasquet, D., Pin, C., 2019. Petrogenesis of the Early-Triassic quartz-monzodiorite dykes from Central Jebilet (Moroccan Meseta): Trace element and Nd-Sr isotope constraints on magma sources, and inferences on their geodynamic context. Journal of African Earth Sciences 149, 451–464. https://doi.org/10.1016/j.jafrearsci.2018.08.023

Boummane, M.H., Olivier, P., 2007. The Oulad Ouaslam Variscan granitic pluton (Jebilets Massif, Southwestern Moroccan Meseta): A forcibly emplaced laccolithic intrusion characterized by its magnetic and magmatic fabrics. Journal of African Earth Sciences 47, 49–61. https://doi.org/10.1016/j.jafrearsci.2006.10.004

Carbonell, R., Simancas, F., Juhlin, C., Pous, J., Pérez-Estaún, A., Gonzalez-Lodeiro, F., Muñoz, G., Heise, W., and Ayarza, P., 2004. Geophysical evidence of a mantle derived

intrusion in SW Iberia. Geophysical Research Letters 31, L11601. https://doi.org/10.1029/2004GL019684.

Chalot-Prat, F., Vachard, D., 1989. Découverte de Foraminifères serpoukhoviens (Namurien inférieur) dans la série volcano-sédimentaire du Tazekka (Maroc oriental). Comptes Rendus de l'Académie des sciences, Série II 308, 1157–1160.

Chalot-Prat, F., 1995. Genesis of rhyolitic ignimbrites and lavas from distinct sources at a deep crustal level: field, petrographic, chemical and isotopic (Sr, Nd) constraints in the Tazekka volcanic complex (Eastern Morocco). Lithos 36, 29–49. https://doi.org/10.1016/0024-4937(95)00004-Y

Chaïeb, 2004. Carte géologique du Maroc au 1/50 000 – Feuille d'Ahfir. Notes et Mémoires du Service Géologique du Maroc 453.

Chelle-Michou, C., Laurent, O., Moyen, J.-F., Block, S., Paquette, J.-L., Couzinié, S., Gardien, V., Vanderhaeghe, O., Villaros, A., Zeh, A., 2017. Pre-Cadomian to late-Variscan odyssey of the eastern Massif Central, France: Formation of the West European crust in a nutshell. Gondwana Research 46, 170–190. https://doi.org/10.1016/j.gr.2017.02.010

Chegham, A., 1985. Etude minéralogique et géologique des filons Pb-Zn-Ag (Fe, Ca, Ba) de Sidi Lahcen (Boutonnière de Mekkam, Maroc oriental). Thèse de 3e cycle, Université d'Orléans, France, 227pp.

Chemsseddoha, A., 1986. Cisaillement ductile et granites syntectoniques dans les Jebilet centrales : L'exemple du pluton hercynien des Oulad-Ouaslam (massif des Jebilet, Meseta Sud-marocaine). Thèse de 3e cycle, Université Rennes 1, 155pp.

Chèvremont P., Cailleux Y., Baudin T., Razin P., Thiéblemont D., Hoepffner C., Bensahal A., Benhaourch R., Carte géologique du Maroc au 1/50 000, feuille d'Ezzhiliga, Mémoire explicatif. Notes et Mémoires du Service Géologique du Maroc 413 bis, 1–93.

Cheilletz, A., Rossi, M., Tarrieu, L., Gasquet, D., Bounajma, H., Mantoy, T., Ouazzani, L., Ouchtouban, L., Deloule, E., Burnard, P., Paquette, J.L., 2015. A cordilleran zoning model for the polymetallic W-Au-Pb-Zn-Ag Tighza-Jbel Aouam District (Central Morocco): contribution from new He-Ar and U-Th-Pb data. Proceedings of the13th SGA meeting, Nancy (France), vol. 4, 1579–1582.

Chopin, F., Corsini, M., Schulmann, K., El Houicha, M., Ghienne, J.-F., Edel, J.-B., 2014. Tectonic evolution of the Rehamna metamorphic dome (Morocco) in the context of the Alleghanian-Variscan orogeny. Tectonics 33, 1154–1177. https://doi.org/10.1002/2014TC003539

Clauer, N., Jeannette, D., Tisserant, D., 1980. Datation isotopique des cristallisations successives d'un socle cristallin et cristallophyllien (Haute Moulouya, Moyen Maroc). Geologische Rundschau 69, 63–83. https://doi.org/10.1007/BF01869024

Costa, S., Rey; P., 1995. Lower crustal rejuvenation and growth during post-thickening collapse: Insights from a crustal cross section through a Variscan metamorphic core complex. Geology 23, 905–908. https://doi.org/10.1130/0091-7613(1995)023<0905:LCRAGD>2.3.CO;2

Corfu, F., Hanchar, J.M., Hoskin, P.W.O., Kinny, P., 2003. Atlas of Zircon Textures. Reviews in Mineralogy and Geochemistry 53, 469–500. https://doi.org/10.2113/0530469

Cózar, P., Vachard, D., Izart, A., Said, I., Somerville, I., Rodríguez, S., Coronado, I., El Houicha, M., Ouarhache, D., 2020. Lower-middle Viséan transgressive carbonates in Morocco: Palaeobiogeographic insights. Journal of African Earth Sciences 168, 103850. https://doi.org/10.1016/j.jafrearsci.2020.103850

Delchini, S., Lahfid, A., Lacroix, B., Baudin, T., Hoepffner, C., Guerrot, C., Lach, P., Saddiqi, O., Ramboz, C., 2018. The Geological Evolution of the Variscan Jebilet Massif, Morocco, Inferred From New Structural and Geochronological Analyses. Tectonics 37, 4470–4493. https://doi.org/10.1029/2018TC005002

Desteucq, C., Hoepffner, C., 1980. Déformations hercyniennes dans les boutonnières paléozoïques de Debdou et du Mekkam. Mines, Géologie et Energie 48, 93–99.
Desteucq, C., Izart, A., Potherat, P., 1988. Etude sédimentologique du Carbonifère du bassin de Jérada (Maroc orienlal). Annales de la Société Géologique du Nord, Lille 107, 203–210.
Diot, H., Bouchez, J.L., 1989. Les granitoïdes hercyniens de la Haute-Moulouya (Maroc): leur structure primaire déduite de l'ASM. Indications sur leur mise en place. Bulletin de la Société Géologique de France 5, 705–716. https://doi.org/10.2113/gssgfbull.v.4.705
Diot, H., Bouchez, J.-L., 1991. Structure des massifs granitiques de la Meseta marocaine, marqueurs géodynamiques : Aouli-Bou-Mia (Haute Moulouya), Zaër (Massif Central) et Sebt de Brikiine (Rehamna). Géologie Méditerranéenne 18, 81–97. https://doi.org/10.3406/geolm.1991.1454
Domeier, M., Font, E., Youbi, N., Davies, J., Nemkin, S., Van der Voo, R., Perrot, M., Benabbou, M., Boumehdi, M.A., Torsvik, T.H., 2021. On the Early Permian shape of Pangea from paleomagnetism at its core. Gondwana Research 90, 171–198. https://doi.org/10.1016/j.gr.2020.11.005
Dostal, J., Keppie, J.D., Hamilton, M.A., Aarab, E.M., Lefort, J.P., Murphy, J.B., 2005. Crustal xenoliths in Triassic lamprophyre dykes in western Morocco: Tectonic implications for the Rheic Ocean suture. Geological Magazine 142(2), 159–172. https://doi.org/10.1017/S0016756805000440
Driouch, Y., Béziat, D., Grégoire, M., Laguenini, F., Ben Abbou, M., Ntarmouchant, A., Roddaz, M., Dahire, M., Bennouna, A., Belkasmi, M., Brusset, S., Debat, P., 2010. Clinopyroxene trace element compositions of cumulate mafic rocks and basalts from the Hercynian Moroccan Central Meseta: Petrogenetic implications. Journal of African Earth Sciences 56, 97–106. https://doi.org/10.1016/j.jafrearsci.2009.05.007
Duchêne, S., Severac, J.-L., Samalens, N., Driouch, Y., Ntarmouchant, A., Kriegsman, L., Dahire, M., Debat, P., Gouy, S., 2022. Multi-stage metamorphism recorded in crustal xenoliths from Permian dykes of the region of Mrirt (Moroccan Central Massif). Journal of African Earth Sciences 194, 104636. https://doi.org/10.1016/J.JAFREARSCI.2022.104636
Edel, J.-B., Schulmann, K., Lexa, O., Diraison, M., Géraud, Y., 2015. Permian clockwise rotations of the Ebro and Corso-Sardinian blocks during Iberian–Armorican oroclinal bending: preliminary paleomagnetic data from the Catalan Coastal Range (NE Spain). Tectonophysics, 657, 172–186. https://doi.org/10.1016/j.tecto.2015.07.002
Edel, J.-B., Schulmann, K., Lexa, O., Lardeaux, J.-M., 2018. Late Palaeozoic palaeomagnetic and tectonic constraints for amalgamation of Pangea supercontinent in the European Variscan belt. Earth-Science Reviews 177, 589–612. https://doi.org/10.1016/j.earscirev.2017.12.007
Eddif, A., Gasquet, D., Hoepffner, C., Levresse, G., 2007. Age of the Wirgane granodiorite intrusions (Western High-Atlas, Morocco): New U–Pb constraints. Journal of African Earth Sciences 47, 227–231. https://doi.org/10.1016/j.jafrearsci.2007.02.003
El Hadi, H., Tahiri, A., Reddad, A., 2003. Les granitoïdes hercyniens post-collisionnels du Maroc oriental : une province magmatique calco-alcaline à shoshonitique. Comptes Rendus Geoscience 335, 959–967. https://doi.org/10.1016/j.crte.2003.09.003
El Hadi, H., Simancas, J.F., Tahiri, A., González-Lodeiro, F., Azor, A., Martínez-Poyatos, D., 2006. Comparative review of the Variscan granitoids of Morocco and Iberia: Proposal of a broad zonation. Geodinamica Acta 19, 103–116. https://doi.org/10.3166/ga.19.103-116
El Houicha, M., Pereira, M.F., Jouhari, A., Gama, C., Ennih, N., Fekkak, A., Ezzouhairi, H., El Attari, A., Silva, J.B., 2018. Recycling of the Proterozoic crystalline basement in the Coastal Block (Moroccan Meseta): New insights for understanding the geodynamic evolution of the northern peri-Gondwanan realm. Precambrian Research 306, 129–154. https://doi.org/10.1016/j.precamres.2017.12.039

El Mouraouah, A.E.A., 1993. Genèse et mise en place des granitoïdes. Cas de la Haute Moulouya (Meseta Orientale, Maroc). Implications géodynamiques. Thèse doctorat ès sciences. Université Cadi Ayyad, Marrakech, Morocco.

El Mouraouah, A.E.A., Diot, H., El Amrani, I., 1993. Les massifs granitiques de la Haute-Moulouya: laccolites granitiques en Meseta marocaine orientale. Comptes Rendus de l'Académie des sciences, Série II 317, 1469–1476.

Elabouyi, M., Dahire, M., Driouch, Y., Duchêne, S., Kriegsman, L.M., Ntarmouchant, A., Kahou, Z.S., Severac, J.L., Belkasmi, M., Debat, P., 2019. Crustal anatexis in the Aouli-Mibladen granitic complex: A window into the middle crust below the Moroccan Eastern Variscan Meseta. Journal of African Earth Sciences 154, 136–163. https://doi.org/10.1016/j.jafrearsci.2019.03.006

Emberger, A., 1965. Introduction à l'étude des minéralisations plombifères de la Haute Moulouya. Notes et Mémoires du Service Géologique du Maroc 181, 167–174.

Erraji, A., 1997. Analyse des terrains carbonifères de la région de Jerada (Maroc oriental) à partir des données de terrain, de forage et de sismique réflexion. Thèse de 3e cycle, Université de Rabat, Morocco, 236pp.

Essaifi, A., Potrel, A., Capdevila, R., Lagarde, J.-L., 2003. Datation U–Pb : Âge de mise en place du magmatisme bimodal des Jebilet centrales (chaîne Varisque, Maroc). Implications géodynamiques. Comptes Rendus Geoscience 335, 193–203. https://doi.org/10.1016/S1631-0713(03)00030-0

Essaifi, A., Samson, S., Goodenough, K., 2014. Geochemical and Sr-Nd isotopic constraints on the petrogenesis and geodynamic significance of the Jebilet magmatism (Variscan Belt, Morocco). Geological Magazine 151, 666–691. https://doi.org/10.1017/S0016756813000654

Essaifi, A., Lacinska, A.M., Corsini, M., Goodenough, K.M., El Arbaoui, A., Zayane, R., 2021. Mobilisation of rare earth elements in shear zones: Insights from the Tabouchent granodioritic pluton (Jebilet massif, Variscan Belt, Morocco). Ore Geology Reviews 133, 103996. https://doi.org/10.1016/j.oregeorev.2021.103996

Ettachfini, E.M., Fekkak, A., Ouanaimi, H., Jouhari, A., Ezzouhairi, H., Ettachfini, M., Hilali, M., Michard, A., 2018. Notice explicative de la carte géologique du Maroc au 1/50 000 – Feuille Azegour, Notes et Mémoires du Service Géologique du Maroc 589 bis.

Faure, M., Monié, P., Pin, C., Maluski, H., Leloix, C., 2002. Late Visean thermal event in the northern part of the French Massif Central: new $^{40}Ar/^{39}Ar$ and Rb–Sr isotopic constraints on the Hercynian syn-orogenic extension. International Journal of Earth Sciences, 91(1), 53–75. https://doi.org/10.1007/s005310100202

Faure, M., Lardeaux, J.-M., Ledru, P., 2009. A review of the pre-Permian geology of the Variscan French Massif Central. Comptes Rendus Geoscience 341, 202–213. https://doi.org/10.1016/j.crte.2008.12.001

Fekkak, A., Ettachfini, E.M., Ouanaimi, H., Toufiq, A., Ezzouhairi, H., Jouhari, A., Company, M., Andreu, B., El Attari, A., Michard, A., 2018. Notice explicative de la carte géologique du Maroc au 1/50 000 – Feuille Addouz, Notes et Mémoires du Service Géologique du Maroc 590 bis.

Filali, F., Guiraud, M., Burg, J.-P., 1999. Petro-structural investigation of the Aouli-Mibladen window (Upper Moulouya): Consequences for Variscan geodynamics in Morocco. Bulletin de la Société Géologique de France 170, 435–450.

Franke, W., 2014. Topography of the Variscan orogen in Europe: Failed-not collapsed. International Journal of Earth Sciences 103, 1471–1499. https://doi.org/10.1007/s00531-014-1014-9

Franke, W., Doublier, M.P., Klama, K., Potel, S., Wemmer, K., 2011. Hot metamorphic core complex in a cold foreland. International Journal of Earth Sciences 100, 753–785. https://doi.org/10.1007/s00531-010-0512-7

Franke, W., Cocks, L.R.M., Torsvik, T.H., 2017. The Palaeozoic Variscan oceans revisited. Gondwana Research 48, 257–284. https://doi.org/10.1016/j.gr.2017.03.005

Fréville, K., Trap, P., Vanardois, J., Melleton, J., Faure, M., Bruguier, O., Poujol, M., Lach, P., 2022. Carboniferous tectono-metamorphic evolution of the Variscan crust in the Belledonne-Pelvoux area. BSGF - Earth Sciences Bulletin 193, 0–67. https://doi.org/10.1051/bsgf/2022008

Frizon De Lamotte, D., Tavakoli-Shirazi, S., Leturmy, P., Averbuch, O., Mouchot, N., Raulin, C., Leparmentier, F., Blanpied, C., Ringenbach, J.C., 2013. Evidence for Late Devonian vertical movements and extensional deformation in northern Africa and Arabia: Integration in the geodynamics of the Devonian world. Tectonics 32, 107–122. https://doi.org/10.1002/tect.20007

Gardien, V., Martelat, J.-E., Leloup, P.H., Mahéo, G., Bevillard, B., Allemand, P., Monié, P., Paquette, J.-L., Grosjean, A.S., Faure, M., Chelle-Michou, C., Fellah, C., 2022. Fast exhumation rate during late orogenic extension: The new timing of the Pilat detachment fault (French Massif Central, Variscan belt). Gondwana Research 103, 260–275. https://doi.org/10.1016/j.gr.2021.10.007

Gasquet, D., Leterrier, J., Mrini, Z., Vidal, P., 1992. Petrogenesis of the Hercynian Tichka plutonic complex (Western High Atlas, Morocco): Trace element and Rb-Sr and Sm-Nd isotopic constraints. Earth and Planetary Science Letters, 108(1–3), 29–44. https://doi.org/10.1016/0012-821X(92)90058-4

Gasquet, D., Stussi, J.M., Nachit, H., 1996. Les granitoïdes hercyniens du Maroc dans le cadre de l'évolution géodynamique régionale. Bulletin de la Société Géologique de France 167, 517–528.

Guardia, P., 1975. Géodynamique de la marge alpine du continent africain d'après l'étude de l'Oranie nord-occidentale : relations structurales et paléogéographiques entre le Rif externe, le Tell et l'avant-pays atlasique. Thèse de 3e cycle, Université de Nice, France.

Gutiérrez-Alonso, G., Fernández-Suárez, J., Weil, A.B., Brendan Murphy, J., Damian Nance, R., Corfú, F., Johnston, S.T., 2008. Self-subduction of the Pangaean global plate. Nature Geoscience, 1(8), 549–553. https://doi.org/10.1038/ngeo250

Gutiérrez-Alonso, G., Fernández-Suárez, J., Jeffries, T.E., Johnston, S.T., Pastor-Galán, D., Murphy, J.B., Franco, M.P., Gonzalo, J.C., 2011. Diachronous post-orogenic magmatism within a developing orocline in Iberia, European Variscides. Tectonics 30, TC5008. https://doi.org/10.1029/2010TC002845

Gutiérrez-Alonso, G., Johnston, S.T., Weil, A.B., Pastor-Galán, D., Fernández-Suárez, J., 2012. Buckling an orogen: The Cantabrian Orocline. GSA Today 22, 4–9. https://doi.org/10.1130/GSATG141A.1

Hadimi, I.; Ait Lahna, A.; Assafar, H.; Tassinari, C.C.G.; Youbi, N.; Boumehdi, M.; Bensalah, M.K.; Gaggero, L.; Mata, J.; Doblas, M. The Post-Collisional Hercynian Volcanism of Rehamna, Western Meseta, Morocco. Mineral Chemistry, Petrology and U-Pb Dating. In: Proceedings of the 2nd International Congress on Permian and Triassic, Casablanca, Morocco, 25–27 April 2018, pp. 33–35.

Hadimi, I., Youbi, N., Lahna, A.A., Bensalah, M.K., Moutbir, O., Mata, J., Doblas, M., Tassinari, C.C.G., Gaggero, L., Basei, M.A.S., Sato, K., Moume, W. El, Boumehdi, M.A., 2021. U–Pb Zircon Geochronological and Petrologic Constraints on the Post-Collisional Variscan Volcanism of the Tiddas-Souk Es-Sebt des Aït Ikko Basin (Western Meseta, Morocco). Minerals 11(10), 1099. https://doi.org/10.3390/min11101099

Hoepffner, C., 1987. La tectonique hercynienne dans l'Est du Maroc. Thèse d'Etat, Université Louis Pasteur, Strasbourg, France, 280pp.

Hoepffner, C., 1994. La zone Midelt-Tazekka-Bsabis, le domaine interne de la chaîne varisque et ses relations avec le Massif hercynien central. Bulletin de l'Institut Scientifique, Rabat 18, 169–191.

Hoepffner, C., Soulaimani, A., Piqué, A., 2005. The Moroccan Hercynides. Journal of African Earth Sciences 43, 144–165. https://doi.org/10.1016/j.jafrearsci.2005.09.002

Hoepffner, C., Houari, M.R., Bouabdelli, M., 2006. Tectonics of the North African Variscides (Morocco, western Algeria): An outline. Comptes Rendus Geoscience 338, 25–40. https://doi.org/10.1016/j.crte.2005.11.003

Hollard, H., Choubert, G., Bronner, G., Marchand, J., Sougy, J., 1985. Carte géologique du Maroc, échelle 1/1 000 000, Notes et Mémoires du Service Géologique du Maroc 260

Houari, M.-R., 2003. Etude structurale de la boutonnière paléozoïque de Tamlelt (Haut Atlas oriental) : sa place dans la chaîne hercynienne du Maroc. Thèse de doctorat, Université Mohammed 1er, Oujda, 353pp.

Huang, Q., Neubauer, F., Liu, Y., Genser, J., Guan, Q., Chang, R., Yuan, S., Yu, S., 2022. Permian-Triassic granites of the Schladming complex (Austroalpine basement): Implications for subduction of the Paleo-Tethys Ocean in the Eastern Alps. Gondwana Research 109, 205–224. https://doi.org/10.1016/j.gr.2022.05.006

Huvelin, P., 1977. Etude géologique et gîtologique du Massif hercynien des Jebilet (Maroc occidental). Notes et Mémoires du Service Géologique du Maroc 232 bis, 1–307.

Huvelin, P., 1983. Plutonisme à Sidi Lahcen (Paléozoïque du Mekkam, région d'Oujda, Maroc oriental) et présence de cornéennes recoupées par des filons à sheelite et wolframite ou à molybdénite. Comptes Rendus de l'Académie des sciences, Série II 297, 57–62.

Huvelin, P., 1992. Le Carbonifère du Tazekka (Maroc): volcanisme, mise en place des granites et des minéralisations en antimoine. Annales de la Société Géologique du Nord (2eme série) 1, 129–133.

Huvelin, P., Mamet, B., 1989. Essai de datation des transgressions et des phénomènes de resédimentation dans le Viséen supérieur - Namurien du Maroc Oriental. Annales de la Société Géologique du Nord 108, 59–67.

Ikenne, M., Souhassou, M., Arai, S., Soulaimani, A., 2017. A historical overview of Moroccan magmatic events along northwest edge of the West African Craton. Journal of African Earth Sciences 127, 3–15. https://doi.org/10.1016/j.jafrearsci.2016.10.002

Izart, A., Beauchamp, J., Vachard, D., Tourani, A.I., Essamani, M., 1997. Stratigraphie séquentielle du Carbonifère inférieur du Haut Atlas central et des Jebilet (Maroc): Un exemple de bassins à turbidites contrôlées par la tectonique. Journal of African Earth Sciences 24, 445–454. https://doi.org/10.1016/S0899-5362(97)00074-2

Jackson, S.E., Pearson, N.J., Griffin, W.L., Belousova, E.A., 2004. The application of laser ablation-inductively coupled plasma-mass spectrometry to in situ U–Pb zircon geochronology. Chemical Geology 211, 47–69. https://doi.org/10.1016/j.chemgeo.2004.06.017

Jesus, A.P., Munhá, J., Mateus, A., Tassinari, C., Nutman, A.P., 2007. The Beja Layered Gabbroic Sequence (Ossa-Morena Zone, Southern Portugal): Geochronology and geodynamic implications. Geodinamica Acta 20, 139–157. https://doi.org/10.3166/ga.20.139-157

Jouhari M., Chopin, F., El Houicha M., Ghienne J.-F., Schulmann, K., Míková, J., Corsini, M., 2022.U–Pb detrital zircon geochronology and source provenance in the Moroccan Meseta (Variscan Belt): a perspective from the Rehamna massif. Journal of African Earth Sciences 194, 104610. https://doi.org/10.1016/j.jafrearsci.2022.104610

Kadziałko-Hofmokl, M., Mazur, S., Werner, T., Kruczyk, J., 2004. Relationships between magnetic and structural fabrics revealed by Variscan basement rocks subjected to heterogeneous deformation - A case study from the Kłodzko Metamorphic Complex, Central Sudetes, Poland, in: Martín-Hernández, F., Lüneburg, C.M., Aubourg, C., Jackson, M. (Eds.), Magnetic Fabric: Methods and Applications, Geological Society, London, Special Publications 238, pp. 475–491. https://doi.org/10.1144/GSL.SP.2004.238.01.24

Kharbouch, F., 1994. Le volcanisme dévono-dinantien du Massif central et de la Meseta orientale. Bulletin de l'Institut Scientifique, Rabat 18, 192–200.

Kharbouch, F., Juteau, T., Treuil, M., Joron, J.L., Pique, A., Hoepffner, C., 1985. Le volcanisme dinantien de la Meseta marocaine nord-occidentale et orientale. Caractères pétrographiques et géochimiques et implications géodynamiques. Sciences Géologiques, Bulletin, Strasbourg 38, 155–163, https://doi.org/10.3406/sgeol.1985.1703

Kuiper, Y.D., Michard, A., Ruellan, E., Holm-Denoma, C.S., Crowley, J.L., 2021. New petrographic and U–Pb geochronology data from the Mazagan Escarpment, offshore Morocco: Support for an African origin. Journal of African Earth Sciences 181, 104249. https://doi.org/10.1016/j.jafrearsci.2021.104249

Lahfid, A., Baidder, L., Ouanaimi, H., Soulaimani, A., Hoepffner, C., Farah, A., Saddiqi, O., Michard, A., 2019. From extension to compression: high geothermal gradient during the earliest Variscan phase of the Moroccan Meseta; a first structural and RSCM thermometric study. European Journal of Mineralogy 31, 695–713. https://doi.org/10.1127/ejm/2019/0031-2882

Lardeaux, J.-M., Schulmann, K., Faure, M., Janoušek, V., Lexa, O., Skrzypek, E., Edel, J.-B., Štípská, P., 2014. The moldanubian zone in the French Massif Central, Vosges/Schwarzwald and Bohemian Massif revisited: differences and similarities. Geological Society, London, Special Publications, 405(1), 7–44. https://doi.org/10.1144/SP405.14

Laurent, O., Couzinié, S., Zeh, A., Vanderhaeghe, O., Moyen, J.-F., Villaros, A., Gardien, V., Chelle-Michou, C., 2017. Protracted, coeval crust and mantle melting during Variscan late-orogenic evolution: U–Pb dating in the eastern French Massif Central. International Journal of Earth Sciences, 106(2), 421–451. https://doi.org/10.1007/s00531-016-1434-9

Lazreq, N., Königshof, P., Essaifi, A., Bouari, A., Outigua, A., 2021. A Devonian age for the Sarhlef Formation (Jebilet Massif, Morocco) – evidence from new biostratigraphic data based on metamorphosed conodonts. Palaeogeography, Palaeoclimatology, Palaeoecology 572, 110395. https://doi.org/10.1016/J.PALAEO.2021.110395

Ledru, P., Courrioux, G., Dallain, C., Lardeaux, J.-M., Montel, J.-M., Vanderhaeghe, O., Vitel, G., 2001. The Velay dome (French Massif Central): melt generation and granite emplacement during orogenic evolution. Tectonophysics, 342(3–4), 207–237. https://doi.org/10.1016/S0040-1951(01)00165-2

Leprêtre, R., Schito, A., Ouchaou, R., El Houicha, M., Chopin, F., 2020. A Pyrenean-like model for the Variscan belt in NW Africa : insights from thermometry-based Raman spectroscopy study in the Khenifra Basin. EGU Gen. Assem. 2020, Online, 4–8 May 2020, EGU2020-20672. https://doi.org/10.5194/egusphere-egu2020-20672

Lucas, G., 1952. Bordure nord des Hautes Plaines dans l'Algérie occidentale. Primaire. Jurassique. Analyse structurale., in: Monographie régionale. 1ère série (Ed.). Alger, p. 139.

Malavieille, J., 1993. Late Orogenic extension in mountain belts: Insights from the basin and range and the Late Paleozoic Variscan Belt. Tectonics 12, 1115–1130. https://doi.org/10.1029/93TC01129

Malavieille, J., Guihot, P., Costa, S., Lardeaux, J.-M., Gardien, V., 1990. Collapse of the thickened Variscan crust in the French Massif Central: Mont Pilat extensional shear zone

and St. Etienne Late Carboniferous basin. Tectonophysics 177, 139–149. https://doi.org/10.1016/0040-1951(90)90278-G

Marcoux, E., Belkabir, A., Gibson, H.L., Lentz, D., Ruffet, G., 2008. Draa Sfar, Morocco: A Visean (331 Ma) pyrrhotite-rich, polymetallic volcanogenic massive sulphide deposit in a Hercynian sediment-dominant terrane. Ore Geology Reviews 33, 307–328. https://doi.org/10.1016/j.oregeorev.2007.03.004

Marcoux, É., Nerci, K., Branquet, Y., Ramboz, C., Ruffet, G., Peucat, J.-J., Stevenson, R., Jébrak, M., 2015. Late-Hercynian intrusion-related gold deposits: An integrated model on the Tighza polymetallic district, central Morocco. Journal of African Earth Sciences 107, 65–88. https://doi.org/10.1016/j.jafrearsci.2015.01.011

Marhoumi, M.R., Hoepffner, C., Doubinger, J., Rauscher, R., 1983. Données nouvelles sur l'histoire hercynienne de la Meseta orientale au Maroc: l'âge dévonien des schistes de Debdou et du Mekkam. Comptes Rendus de l'Académie des sciences, Série II 297, 69–72.

Marhoumi, R., Rauscher, R., 1984. Un plancton dévonien de la meseta orientale au Maroc. Review of Palaeobotany and Palynology 43, 237–253. https://doi.org/10.1016/0034-6667(84)90035-6

Martínez-Catalán, J.R., Pascual, F.J.R., Montes, A.D., Fernández, R., Barreiro, J.G., Da Silva, Í.D., Clavijo, E.G., Ayarza, P., Alcock, J.E., 2014. The late variscan HT/LP metamorphic event in NW and Central Iberia: Relationships to crustal thickening, extension, orocline development and crustal evolution. Geological Society, London, Special Publications 405, 225–247. https://doi.org/10.1144/SP405.1

Martínez-Catalán, J.R., Schulmann, K., Ghienne, J.-F., 2021. The Mid-Variscan Allochthon: Keys from correlation, partial retrodeformation and plate-tectonic reconstruction to unlock the geometry of a non-cylindrical belt. Earth-Science Reviews 220. https://doi.org/10.1016/j.earscirev.2021.103700

Médioni, R., 1980. Mise au point stratigraphique sur les terrains carbonifères de la bordure septentrionale des Hauts-Plateaux marocains (Massif de Debdou, boutonnières de Lalla-Mimouna et du Mekkam). Notes et Mémoires du Service Géologique du Maroc 285, 25–37.

Michard, A., 1976. Eléments de géologie marocaine. Notes et Mémoires du Service Géologique du Maroc 252, 1−408.

Michard, A, Hoepffner, C., Soulaimani, A., Baidder, L., 2008. The Variscan Belt, in: Michard, André, Saddiqi, O., Chalouan, A., Lamotte, D. de (Eds.), Continental Evolution: The Geology of Morocco. Springer Berlin Heidelberg, pp. 65–132. https://doi.org/10.1007/978-3-540-77076-3_3

Michard, A., Soulaimani, A., Hoepffner, C., Ouanaimi, H., Baidder, L., Rjimati, E.C., Saddiqi, O., 2010. The South-Western Branch of the Variscan Belt: Evidence from Morocco 492, 1–24. Tectonophysics. https://doi.org/10.1016/j.tecto.2010.05.021

Moreno, C., Sáez, R., González, F., Almodóvar, G., Toscano, M., Playford, G., Alansari, A., Rziki, S., Bajddi, A., 2008. Age and depositional environment of the Draa Sfar massive sulfide deposit, Morocco. Mineralium Deposita 43, 891–911. https://doi.org/10.1007/s00126-008-0199-x

Mrini, Z., Rafi, A., Duthou, J.L., Vidal, P., 1992. Chronologie Rb-Sr des granitoïdes hercyniens du Maroc : conséquences. Bulletin de la Société Géologique de France 163, 281–291.

Muratet, B., 1995. Carte géologique du Maroc : Taourirt - Echelle 1/100 000. Notes et Mémoires du Service Géologique du Maroc 364.

Najih, A., Montero, P., Verati, C., Chabou, M.C., Fekkak, A., Baidder, L., Ezzouhairi, H., Bea, F., Michard, A., 2019. Initial Pangean rifting north of the West African Craton: Insights from late Permian U-Pb and $^{40}Ar/^{39}Ar$ dating of alkaline magmatism from the

Eastern Anti-Atlas (Morocco). Journal of Geodynamics 132, 101670. https://doi.org/10.1016/j.jog.2019.101670

Nemchin, A.A., Cawood, P.A., 2005. Discordance of the U–Pb system in detrital zircons: Implication for provenance studies of sedimentary rocks. Sedimentary Geology 182, 143–162. https://doi.org/10.1016/J.SEDGEO.2005.07.011

Ouabid, M., Ouali, H., Garrido, C.J., Acosta-Vigil, A., Román-Alpiste, M.J., Dautria, J.M., Marchesi, C., Hidas, K., 2017. Neoproterozoic granitoids in the basement of the Moroccan Central Meseta: Correlation with the Anti-Atlas at the NW paleo-margin of Gondwana. Precambrian Research 299, 34–57. https://doi.org/10.1016/J.PRECAMRES.2017.07.007

Ouabid, M., Garrido, C.J., Ouali, H., Harvey, J., Hidas, K., Marchesi, C., Acosta-Vigil, A., Dautria, J.-M., El Messbahi, H., Román-Alpiste, M.J., 2021. Late Cadomian rifting of the NW Gondwana margin and the reworking of Precambrian crust – evidence from bimodal magmatism in the early Paleozoic Moroccan Meseta. International Geology Review 63(16), 2013–2036. https://doi.org/10.1080/00206814.2020.1818301

Ouanaimi, H., Fekkak, A., Ettachfini, E.M., El Arabi, A., Jouhari, A., Ezzouhairi, H., Lagnaoui, A., Hilali, M., Michard, A., 2018. Carte Géologique du Maroc au 1/50000, Feuille Amezmiz- Notice explicative. Notes et Mémoires du Service Géologique du Maroc, Rabat 588bis.

Oukemeni D., Bourne J.H. 1993, Etude géochimique des granitoïdes du pluton d'Aouli, Haute Moulouya, Maroc. Journal of African Earth Sciences (and the Middle East) 17, 429–443. https://doi.org/10.1016/0899-5362(93)90002-8

Oukemeni, D., Bourne, J., Krogh, T.E., 1995. Géochronologie U–Pb sur zircon du pluton d'Aouli, Haute Moulouya, Maroc. Bulletin de la Société Géologique de France 166, 15–21.

Owodenko, B., 1976. Le Bassin houiller de Jerada (Maroc oriental), essai de synthèse et de paléogéographie, Notes et Mémoires du Service Géologique du Maroc 207 bis.

Pereira, M.F., El Houicha, M., Aghzer, A., Silva, J.B., Linnemann, U., Jouhari, A., 2014. New U-Pb zircon dating of late Neoproterozoic magmatism in Western Meseta (Morocco). Gondwana 15. North meets South. 133.

Pereira, M.F., Castro, A., Fernández, C., 2015a. The inception of a Paleotethyan magmatic arc in Iberia. Geoscience Frontiers 6, 297–306. https://doi.org/10.1016/j.gsf.2014.02.006

Pereira, M.F., El Houicha, M., Chichorro, M., Armstrong, R., Jouhari, A., El Attari, A., Ennih, N., Silva, J.B., 2015b. Evidence of a Paleoproterozoic basement in the Moroccan Variscan Belt (Rehamna Massif, Western Meseta). Precambrian Research 268, 61–73. https://doi.org/10.1016/j.precamres.2015.07.010

Pereira, M.F., Díez Fernández, R., Gama, C., Hofmann, M., Gärtner, A., Linnemann, U., 2018. S-type granite generation and emplacement during a regional switch from extensional to contractional deformation (Central Iberian Zone, Iberian autochthonous domain, Variscan Orogeny). International Journal of Earth Sciences 107, 251–267. https://doi.org/10.1007/s00531-017-1488-3

Pereira, M.F., Dias da Silva, Í., Rodríguez, C., Corfu, F., Castro, A., 2023. Visean high-K mafic-intermediate plutonic rocks of the Ossa-Morena Zone (SW Iberia): implications for regional extensional tectonics. Geological Society, London, Special Publications 531. https://doi.org/10.1144/SP531-2022-118

Piqué, A., 1979. Evolution structurale d'un segment de la chaîne hercynienne: la Meseta nord-occidentale. Sciences Géologiques, Mémoires 56, 243.

Pin, C., Paquette, J.-L., 2002. Le magmatisme basique calcoalcalin d'âge dévono-dinantien du nord du Massif Central, témoin d'une marge active hercynienne : arguments géochimiques et isotopiques Sr/Nd. Sr-Nd isotope and trace element evidence for a Late Devonian active

margin in northern Massif-Central (France). Geodinamica Acta, 15(1), 63−77. https://doi.org/10.1080/09853111.2002.10510739

Piqué, A., Michard, A., 1989. Morrocan Hercynides: a synopsis. The Paleozoic sedimentary and tectonic evolution at the northern margin of West Africa. American Journal of Science 289, 286−330. https://doi.org/10.2475/ajs.289.3.286

Playford, G., González, F., Moreno, C., Al Ansari, A., 2008. Palynostratigraphy of the Sarhlef Series (Mississippian), Jebilet Massif, Morocco. Micropaleontology 54, 89–124.

Poilvet, J.C., Poujol, M., Pitra, P., Van Den Driessche, J. and Paquette, J.L., 2011. The Montalet granite, Montagne Noire, France: An Early Permian syn-extensional pluton as evidenced by new U-Th-Pb data on zircon and monazite. Comptes Rendus Geoscience, 343(7), 454-461. https://doi.org/10.1016/j.crte.2011.06.002

Pouclet, A., El Hadi, H., Bardintzeff, J.M., Benharref, M., Fekkak, A., 2017. Devonian to Early Carboniferous magmatic alkaline activity in the Tafilalt Province, Eastearn Morocco: An Eovariscan episode in the Gondwana margin, north of the West African Craton. Journal of African Earth Sciences 129, 814–841. https://doi.org/10.1016/j.jafrearsci.2017.01.030

Poujol, M., Pitra, P., Van Den Driessche, J., Tartèse, R., Ruffet, G., Paquette, J.-L., Poilvet, J.C., 2017. Two-stage partial melting during the Variscan extensional tectonics (Montagne Noire, France). International Journal of Earth Sciences 106, 477–500. https://doi.org/10.1007/s00531-016-1369-1

Rafi, A., 1988. Approche pétrographique, géochimique et géochronologique (Rb-Sr) des granitoïdes du Maroc Oriental. Thèse de 3e cycle, Université de Marrakech, Morocco.

Remaci-Benaouda, N., 2005. Pétrologie et géochimie des associations 'felsique-mafique' tardi-hercyniennes oranaises (Algérie Nord occidentale). Implications pétrogénétiques et géodynamiques. Thèse d'Etat, Université d'Es-Sénia, Oran, 229pp.

Ribeiro, M.L., Castro, A., Almeida, A., Menéndez, L.G., Jesus, A., Lains, J.A., Lopes, J.C., Martins, H.C.B., Mata, J., Mateus, A., Moita, P., Neiva, A.M.R., Ribeiro, M.A., Santos, J.F., Solá, A.R., 2019. The Geology of Iberia: A Geodynamic Approach. Variscan Magmatism 497–526. https://doi.org/10.1007/978-3-030-10519-8_13

Roddaz, M., Brusset, S., Soula, J.-C., Béziat, D., Ben Abbou, M., Debat, P., Driouch, Y., Christophoul, F., Ntarmouchant, A., Déramond, J., 2002. Foreland basin magmatism in the Western Moroccan Meseta and geodynamic inferences. Tectonics 21, 1043. https://doi.org/10.1029/2001TC901029

Rolin, P., Marquer, D., Colchen, M., Cartannaz, C., Cocherie, A., Thiery, V., Quenardel, J.M., Rossi, P., 2009. Famenno-carboniferous (370-320 Ma) strike slip tectonics monitored by syn-kinematic plutons in the French Variscan belt (Massif Armoricain and French Massif Central). Bulletin de la Société Géologique de France 180, 231–246. https://doi.org/10.2113/gssgfbull.180.3.231

Rosé, F., 1987. Les types granitiques du Maroc hercynien. Thèse d'Etat, Université Paris VI, France, 381pp.

Rossi, M., Tarrieu, L., Cheilletz, A., Gasquet, D., Deloule, E., Paquette, J.-L., Bounajma, H., Mantoy, T., Ouazzani, L., Ouchtouban, L., 2016. The polymetallic (W-Au/Pb-Zn-Ag) Tighza district (central Morocco): age of the magmatic and hydrothermal events. In: Bouabdellah, M., Slack, J.F. (Eds.), Mineral deposits of North Africa. Springer-Verlag, Berlin-Heidelberg, pp 107–131. https://doi.org/10.1007/978-3-319-31733-5_3

Rossi, M., Gasquet, D., Cheilletz, A., Tarrieu, L., Bounajma, H., Mantoy, T., Reisberg, L., Deloule, E., Boulvais, P., Burnard, P., 2017. Isotopic and geochemical constraints on lead and fluid sources of the Pb-Zn-Ag mineralization in the polymetallic Tighza-Jbel Aouam district (central Morocco), and relationships with the geodynamic context. Journal of African Earth Sciences, 127, 194–210. https://doi.org/10.1016/j.jafrearsci.2016.08.011

Ruíz Reig, P., 2001. Carte géologique du Maroc au 1/50 000 – Feuille de Berkane, Notes et Mémoires du Service Géologique du Maroc 425.

Schaltegger, U., Fanning, C.M., Günther, D., Maurin, J.C., Schulmann, K., Gebauer, D., 1999. Growth, annealing and recrystallization of zircon and preservation of monazite in high-grade metamorphism: conventional and in situ U–Pb isotope, cathodoluminiscence and microchemical evidence. Contributions to Mineralogy and Petrology 134, 186–201. https://doi.org/10.1007/s004100050478

Schulmann, K., Edel, J.B., Martínez Catalán, J.R., Mazur, S., Guy, A., Lardeaux, J.M., Ayarza, P., Palomeras, I., 2022. Tectonic evolution and global crustal architecture of the European Variscan belt constrained by geophysical data. Earth-Science Reviews 234, 104195. https://doi.org/10.1016/J.EARSCIREV.2022.104195

Simancas, J. F., Carbonell, R., González Lodeiro, F., Pérez Estaún, A., Juhlin, C., Ayarza, P., Kashubin, A., Azor, A., Martıìnez Poyatos, D., Almodóvar, G. R., Pascual, E., Sáez, R., and Expósito, I., 2003. Crustal structure of the trans pressional Variscan orogen of SW Iberia: SW Iberia deep seismic reflection profile (IBERSEIS). Tectonics 22, 1062. https://doi.org/10.1029/2002TC001479

Simancas, J.F., Tahiri, A., Azor, A., Lodeiro, F.G., Martínez Poyatos, D.J., El Hadi, H., 2005. The tectonic frame of the Variscan-Alleghanian orogen in southern Europe and northern Africa. Tectonophysics 398, 181–198. https://doi.org/10.1016/j.tecto.2005.02.006

Simancas, J. F., Carbonell, R., González Lodeiro, F., Pérez Estaún, A., Juhlin, C., Ayarza, P., Kashubin, A., Azor, A., Martıìnez Poyatos, D., Sáez, R., Almodóvar, G. R., Pascual, E., Flecha, I., and Martí, D., 2006. Transpressional collision tectonics and mantle plume dynamics: the Variscides of southwestern Iberia. In: European Lithosphere Dynamics, edited by: Gee, F. G. and Stephensin, R. A., Geological Society, London, Memoirs 32, 345–354. https://doi.org/10.1144/GSL.MEM.2006.032.01.21.

Simancas, J.F., Azor, A., Martínez-Poyatos, D., Tahiri, A., El Hadi, H., González-Lodeiro, F., Pérez-Estaún, A., Carbonell, R., 2009. Tectonic relationships of Southwest Iberia with the allochthons of Northwest Iberia and the Moroccan Variscides. Comptes Rendus Geoscience 341, 103–113. https://doi.org/10.1016/j.crte.2008.11.003

Sláma, J., Kosler, J., Condon, D.J., Crowley, J.L., Gerdes, A., Hanchar, J.M., Horstwood, M.S.A., Morris, G.A., Nasdala, L., Norberg, N., Schaltegger, U., Schoene, B., Tubrett, M.N., Whitehouse, M.J., 2008. Plesovice zircon - A new natural reference material for U–Pb and Hf isotopic microanalysis. Chemical Geology 249, 1–35. https://doi.org/10.1016/j.chemgeo.2007.11.005

Spencer, C.J., Kirkland, C.L., Taylor, R.J.M., 2016. Strategies towards statistically robust interpretations of in situ U–Pb zircon geochronology. Geoscience Frontiers 7, 581–589. https://doi.org/10.1016/J.GSF.2015.11.006

Stampfli, G.M., Vavassis, I., De Bono, A., Rosselet, F., Matti, B., Bellini, M., 2003. Remnants of the paleotethys oceanic suture-zone in the western tethyan area. Bollettino della Società geologica italiana 2, 1–23.

Stampfli, G.M., Hochard, C., Vérard, C., Wilhem, C., 2013. The formation of Pangea. Tectonophysics, 593, 1–19. https://doi.org/10.1016/j.tecto.2013.02.037

Tahiri, A., Montero, P., El Hadi, H., Martínez Poyatos, D., Azor, A., Bea, F., Simancas, J.F., González Lodeiro, F., 2010. Geochronological data on the Rabat-Tiflet granitoids: Their bearing on the tectonics of the Moroccan Variscides. Journal of African Earth Sciences 57, 1–13. https://doi.org/10.1016/j.jafrearsci.2009.07.005

Taki, Z., 2012. Styles structuraux du front nord du Haut Atlas et ces bassins d'avant pays, PhD thesis, Université Ibn Tofail, Kenitra, Maroc.

Tisserant, D., 1977. Les isotopes du strontium et l'histoire hercynienne du Maroc. Etude de quelques massifs atlasiques et mésétiens. Thèse de 3e cycle, Université Louis Pasteur, Strasbourg, France, 103pp.

Torbi, A., 1996. Stratigraphie et évolution structurale paléozoïque d'un segment de la Meseta orientale marocaine (Monts du Sud-Est d'Oujda): Rôle des décrochements dans la formation de l'olistostrome intraviséen et le plutonisme tardi-hercynien. Journal of African Earth Sciences 22, 549–563. https://doi.org/10.1016/0899-5362(96)00036-X

Vanderhaeghe, O., Burg, J.-P., Teyssier, C., 1999. Exhumation of migmatites in two collapsed orogens: Canadian Cordillera and French Variscides, in: Ring, U., Brandon Mark, T., Lister Gordon, S., Willett Sean, D. (Eds Geological Society, London, Special Publications 154, pp. 181–204. https://doi.org/10.1144/GSL.SP.1999.154.01.08

Vanderhaeghe, O., Laurent, O., Gardien, V., Moyen, J.-F., Gébelin, A., Chelle-Michou, C., Couzinié, S., Villaros, A., Bellanger, M., 2020. Flow of partially molten crust controlling construction, growth and collapse of the Variscan orogenic belt: The geologic record of the French Massif Central. BSGF - Earth Sciences Bulletin 191. https://doi.org/10.1051/bsgf/2020013

Vauchez, A., 1976. Les déformations anté-triasiques dans la boutonnière d'Aouli-Mibladen (Midelt-Maroc). Comptes Rendus de l'Académie des sciences, Paris, série D 282, 425–428.

Vermeesch, P., 2018. IsoplotR: A free and open toolbox for geochronology. Geoscience Frontiers 9, 1479–1493. https://doi.org/10.1016/J.GSF.2018.04.001

Weil, A.B., Gutiérrez-Alonso, G., Johnston, S.T., Pastor-Galán, D., 2013. Kinematic constraints on buckling a lithospheric-scale orocline along the northern margin of Gondwana: A geologic synthesis. Tectonophysics 582, 25–49. https://doi.org/10.1016/j.tecto.2012.10.006

Wernert, P., Schulmann, K., Chopin, F., Štípská, P., Bosch, D., El Houicha, M., 2016. Tectonometamorphic evolution of an intracontinental orogeny inferred from P–T–t–d paths of the metapelites from the Rehamna massif (Morocco). Journal of Metamorphic Geology 34, 917–940. https://doi.org/10.1111/jmg.12214

Wiedenbeck, M., Allé, P., Corfu, F., Griffin, W.L., Meier, M., Oberli, F., Von Quadt, A., Roddick, J.C., Spiegel, W., 1995. Three natural zircon standards for U-Th-Pb, Lu-Hf, trace element and REE analyses. Geostandard Newsletter 19, 1–23. https://doi.org/10.1111/j.1751-908X.1995.tb00147.x

Xia, L., Li, X., 2019. Basalt geochemistry as a diagnostic indicator of tectonic setting. Gondwana Research 65, 43–67. https://doi.org/10.1016/j.gr.2018.08.006

Youbi, N.; Gaggero, L.; Assafar, H.; Hadimi, I.; Boumehdi, M.A.; Bensalah, M.K.; Linnemann, U.; Gaertner, A.; Mata, J.; Doblas, M.; et al. U-Pb Zircon Geochronological and Petrologic Constraints on the Post Collisional Variscan Volcanism of the Khénifra Basin (Western Meseta, Morocco): Stratigraphic and Petrogenetic Implications. In Proceedings of the 2nd International Congress on Permian and Triassic, Casablanca, Morocco, 25–27 April 2018, pp. 53–54.

Ziegler, P.A., Dèzes, P., 2006. Crustal evolution of Western and Central Europe. Geological Society, London, Memoirs 32, 43–56. https://doi.org/10.1144/GSL.MEM.2006.032.01.03

Zimmermann, S., Mark, C., Chew, D., Voice, P.J., 2018. Maximising data and precision from detrital zircon U–Pb analysis by LA-ICPMS: The use of core-rim ages and the single-analysis concordia age. Sedimentary Geology 375, 5–13. https://doi.org/10.1016/j.sedgeo.2017.12.020

Žák, J., Verner, K., Janoušek, V., Holub, F.V., Kachlík, V., Finger, F., Hajná, J., Tomek, F., Vondrovic, L., Trubač, J., 2104. A plate-kinematic model for the assembly of the Bohemian Massif constrained by structural relationships around granitoid plutons.

Geological Society, London, Special Publications 405, 169–96.
https://doi.org/10.1144/SP405.9

Figures

Figure 1. Geological map of the Northwest African Variscides in NW Algeria and Morocco (adapted from Hollard et al., 1985- Geol. Map of Morocco). Abbreviations: AB: Azrou Basin; Bdf : Boudoufoud; DB: Debdou-Mekkam; FB: Fourhal Basin; GR: Ghar Roubbane; Gsa: Guemassa; KB: Khenifra-Azrou Basin; Mr: Merguechoum ; SAF: South Atlas Front; SB: Sidi Bettache Basin; SMF: South Meseta Fault Zone; SMFr: South Meseta Front; SMZ: South Meseta Zone; SVDF: South Variscan Deformation Front; TBBFZ: Tazekka-Bsabbis-Berkit Fault Zone; Tn: Tanncherfi ; WHA: Western High Atlas; WMSZ: West Meseta Shear Zone; Za: Zaian Massif; Zek: Zekkara.

Figure 2. Geological map of (a) the Jebilet massif (modified after from Huvelin, 1977; Delchini et al., 2018), (b) the High Moulouya massif (modified after Emberger, 1965) and the Palaeozoic inliers from the Horsts belt in Eastern Meseta (modified after Hollard et al., 1985).

Figure 3. Kernel density plots, Th/U values, probability density plots of concordant $^{206}Pb/^{238}U$ dates (from 250 to 500 Ma), Tera-Wasserburg diagrams and selection of CL images of zircons from the Oulad Ouaslam granodiorite (Jebilet massif).

Figure 4. Kernel density plots, Th/U values, probability density plots of concordant $^{206}Pb/^{238}U$ dates (from 250 to 500 Ma), Tera-Wasserburg diagrams and selection of CL images of zircons from the High Moulouya massif.

Figure 5. Kernel density plots, Th/U values, probability density plots of concordant $^{206}Pb/^{238}U$ dates (from 250 to 500 Ma), Tera-Wasserburg diagrams and selection of CL images of zircons from the Beni Snassen massif and the Horsts belt.

Figure 6. Compilation of available U–Pb and $^{40}Ar/^{39}Ar$ geochronological ages from magmatic rocks in the Meseta, see Table 1. References: 1. Aït Lahna et al. (2018); 2. Baudin et al. (2001), 3. Baudin et al. (2003); 4. Chevrement et al. (2001); 5. Chopin et al. (2014); 6. Delchini et al. (2018); 7. Domeier et al. (2021); 8. Essaifi et al. (2003); 9. Ettachfini et al. (2018); 10. Fekkak et al. (2018); 11. Hadimi et al. (2018) in Domeier et al. (2021); 12 Hadimi et al. (2021); 13. Marcoux et al. (2008); 14. Oukemini et al. (1995); 15. Remaci-Benaouda (2005); 16. Tahiri et al. (2010); 17. Watanabe (2002); 18. Youbi et al. (2018) in Domeier et al. (2021).

Figure 7. Probability density plots of available U–Pb geochronological ages from the French Massif Central (FMC), Iberia and Meseta. Data from the French Massif Central have been extracted from Vanderhaeghe et al. (2020). Data from Iberia have been extracted from Jesus et al. (2007), Martínez-Catalán et al. (2014), Pereira et al. (2018) and Ribeiro et al. (2019). Data

from the FMC and Iberia can be found in Supplementary material 5. Data from the Meseta can be found in Table 1.

Figure 8. Magmatism (early arc magmatism and granitoids) in the Northwest African and Western European Variscan belt. Modified after Martínez-Catalán et al. (2021) and Schulmann et al, (2022). Lithotectonic zones: Central Iberian zone (CIZ); Ossa-Morena zone (OMZ), South Portuguese zone (SPZ); Galicia-Trás-os-Montes zone (GTMZ); West Asturian-Leonese Zone (WALTZ); Cantabrian Zone (CZ). Granitoïds complex from the Meseta: Western High Atlas (WHA); Sebt Brikiine granites (Sbr.); Jebilet intrusions (Jeb.); Oulmès (Oul); Zaër (Zar); Boudoufoud (Bdf); Merguechoum (Mr); Zekkara (Zek); Tiffrit-Saïda (TS). Main shear zones in the Meseta: South Meseta Front (SMFr); West Meseta Shear Zone (WMSZ); Tazekka-Bsabbis-Berkit Fault Zone (TBBFZ).

Figure 9. Paleogeographic reconstruction showing the contrasting tectonic context of the development of the variscan magmatism. Early Carboniferous reconstruction modified after after Martínez-Catalán et al. (2021). Late Carboniferous and early Permian reconstructions modified after Chopin et al. (2014) and Edel et al. (2018).

Table

Table 1. Available geochronological ages from magmatic rocks of the Meseta.

Auxilliary material

Auxilliary material 1. Description of the samples/lithologies

Auxilliary material 2. U–Pb isotopic data on zircon for the Jebilet massif.

Auxilliary material 3. U–Pb isotopic data on zircon for the High Moulouya massif.

Auxilliary material 4. U–Pb isotopic data on zircon for the Horsts belt.

Auxiliary material 5. Compilation of U–Pb and $^{40}Ar/^{39}Ar$ ages of igneous rocks from the French Massif central (extracted and modified after Vanderhaege et al. [2020]) and Iberia (extracted and modified after Jesus et al. [2007], Martínez Catalán et al. [2014], Pereira et al. [2018] and Ribeiro et al. [2019]).

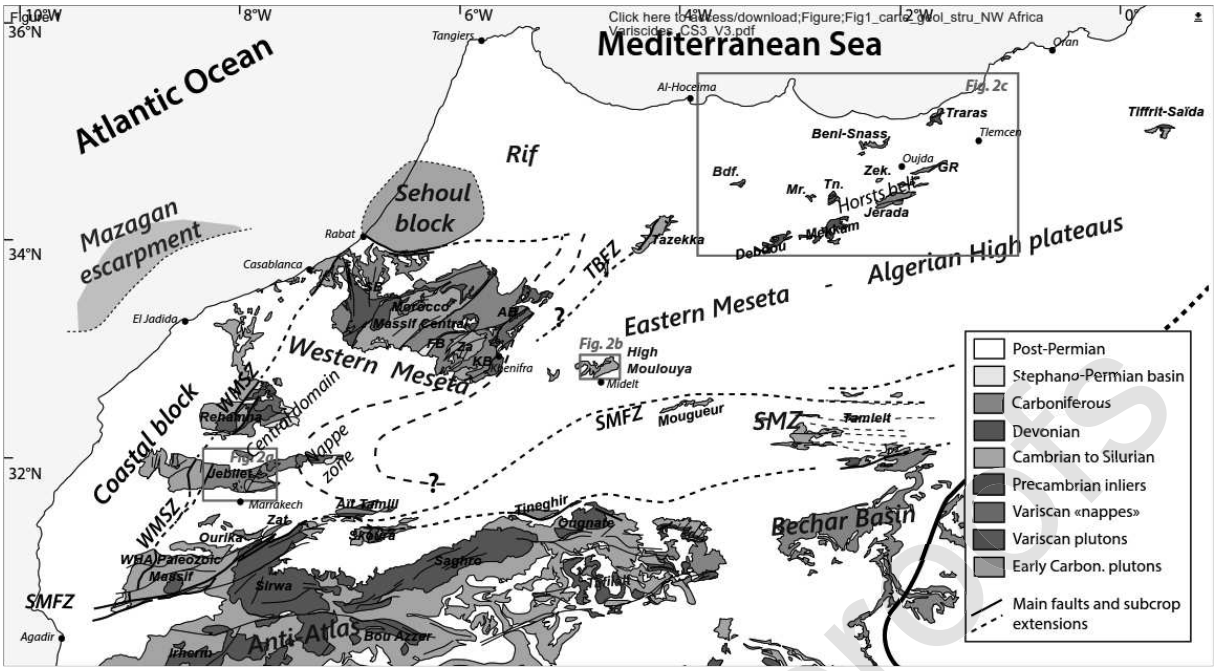

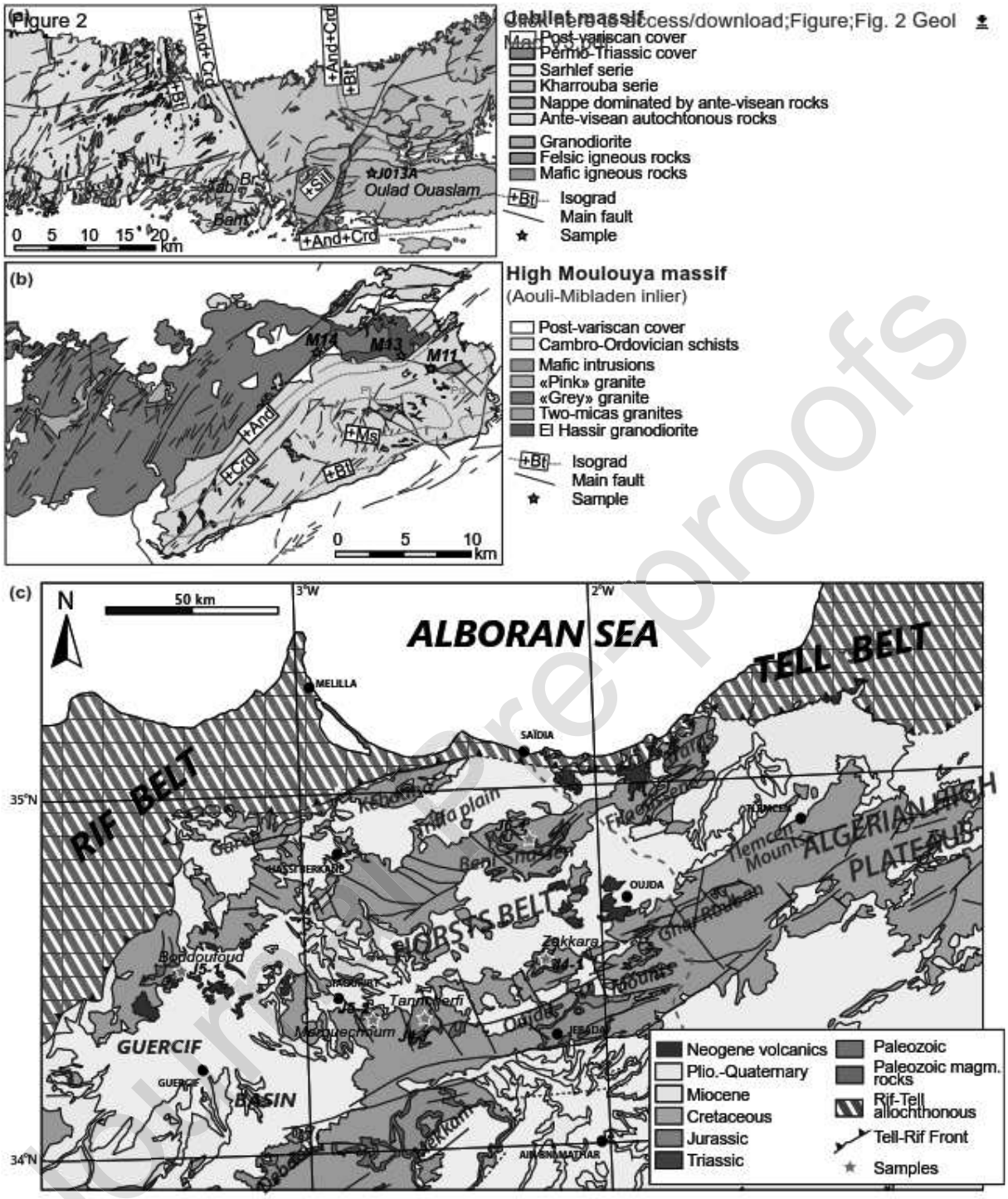

Figure 3

Click here to access/download;Figure;Fig. 3 Jebilet.pdf

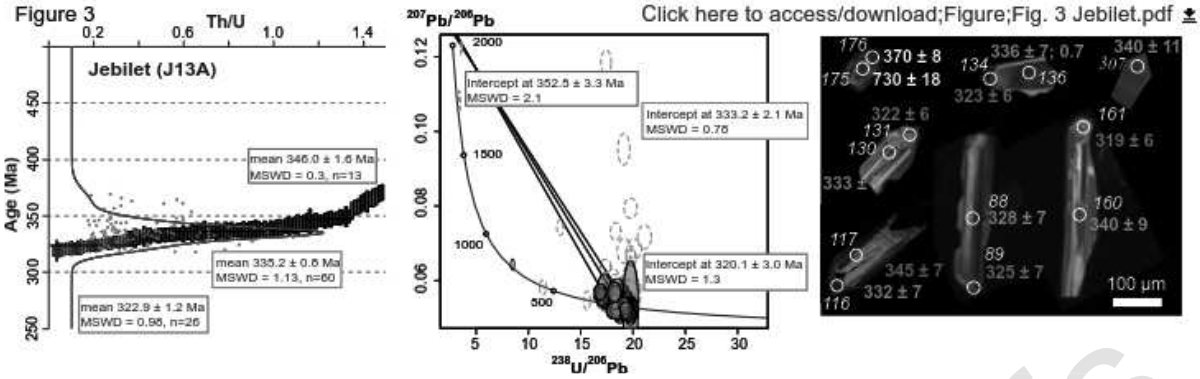

Figure 4

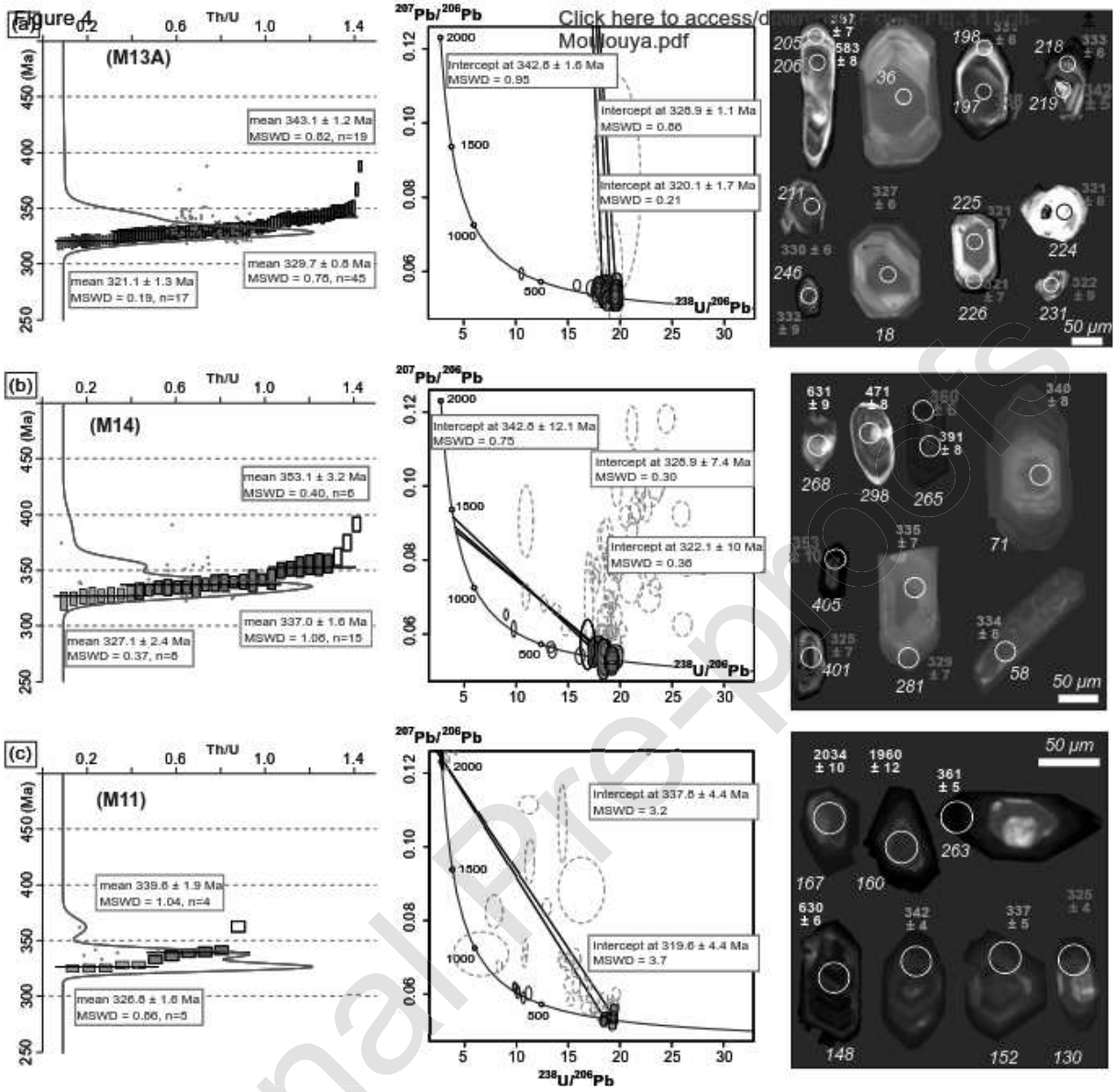

Figure 5 Click here to access/download;Figure;Fig. 5 Horst-Belt.pdf

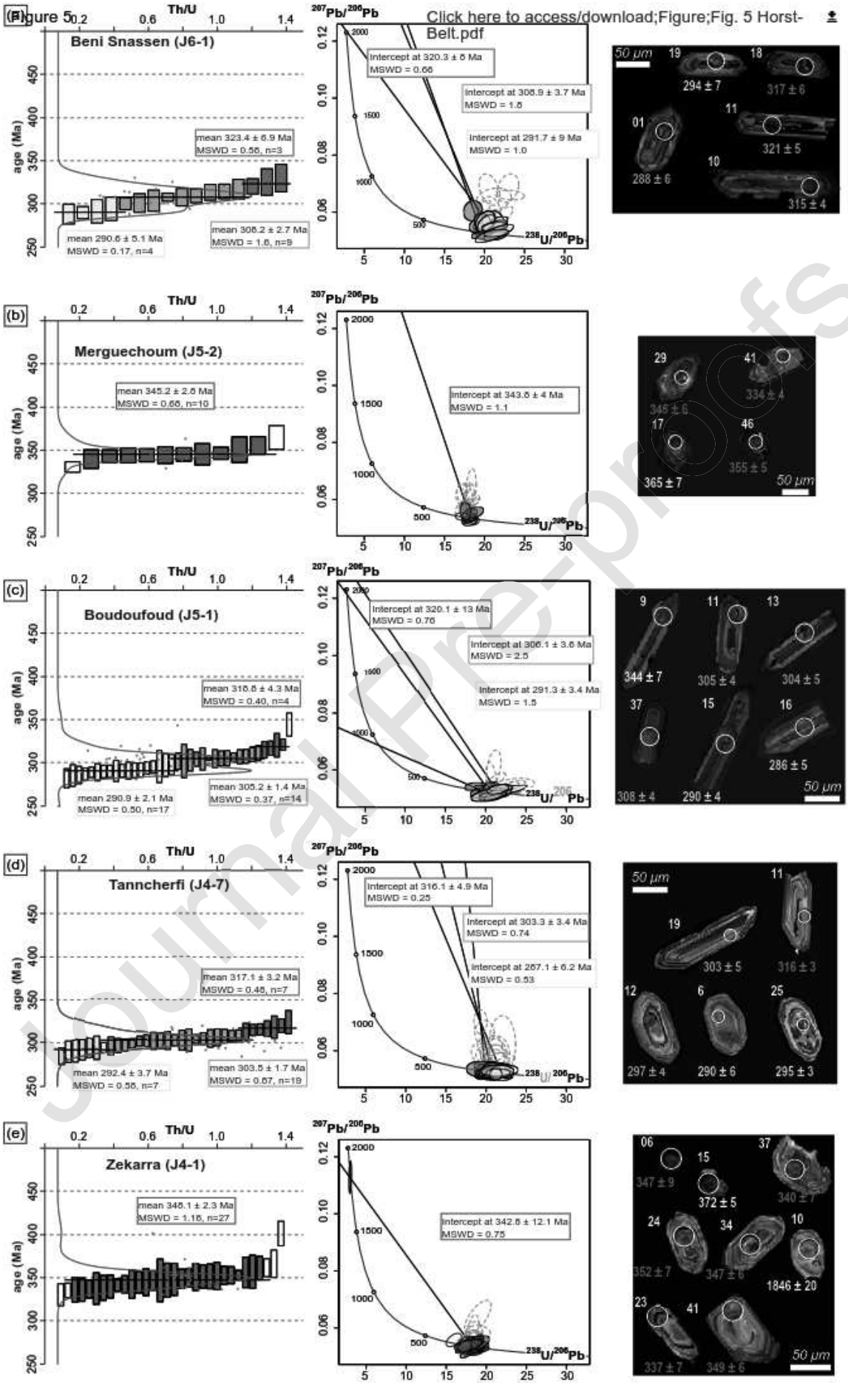

Figure 6

Click here to access/download;Figure;Fig. 6 Synthese_220206_V8.pdf

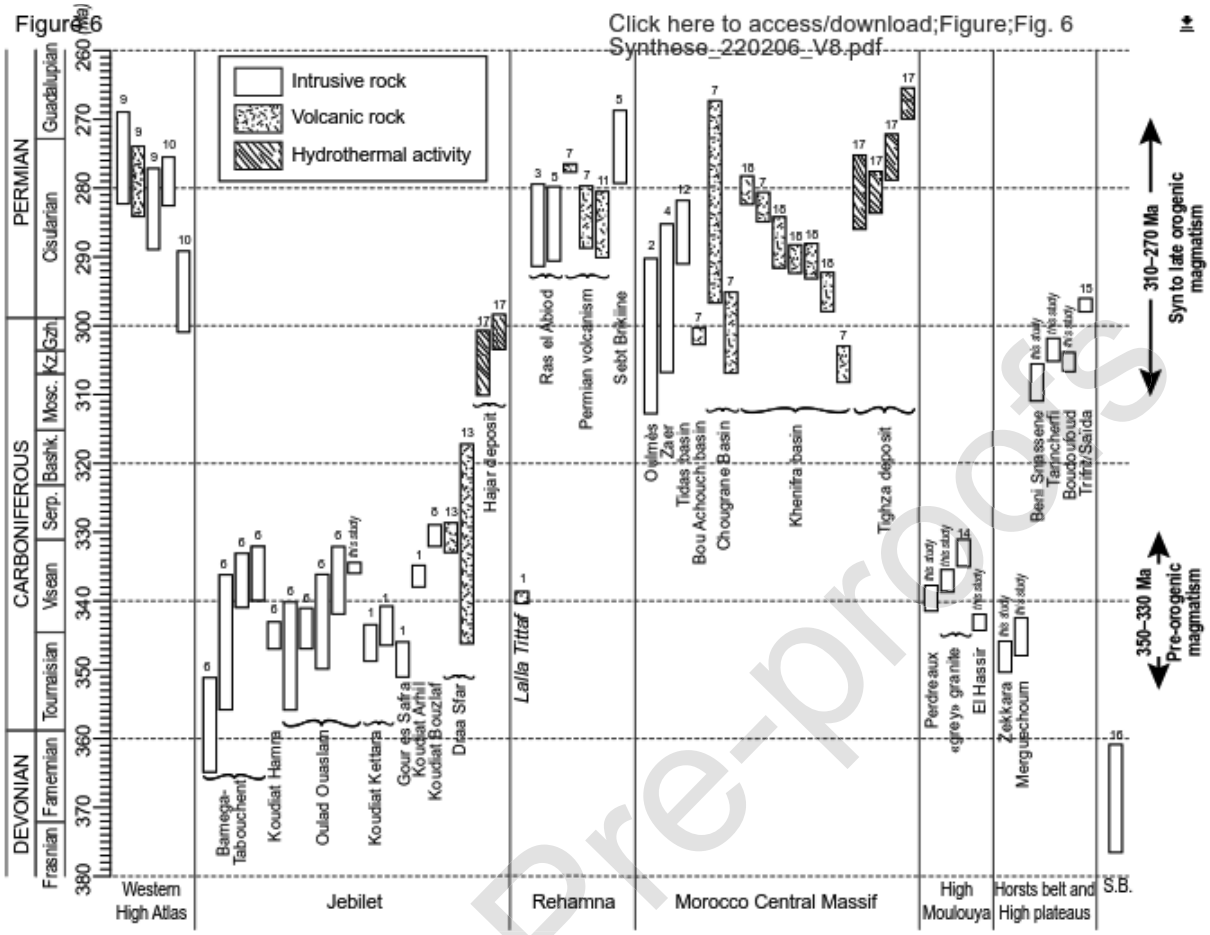

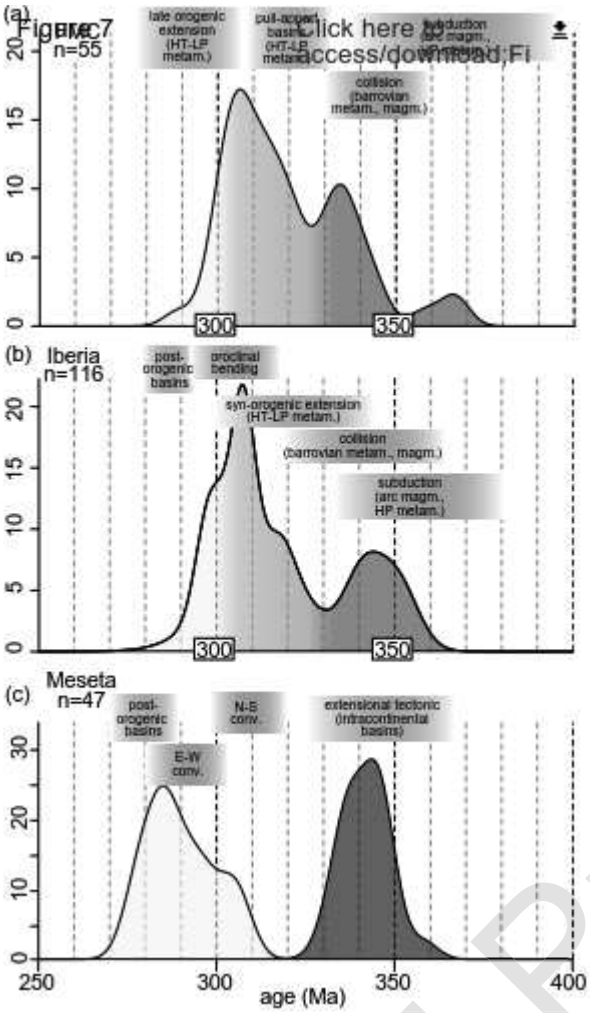

Figure 8

Click here to access/download;Figure;Fig. 8 Granitoid map V15-01.jpg

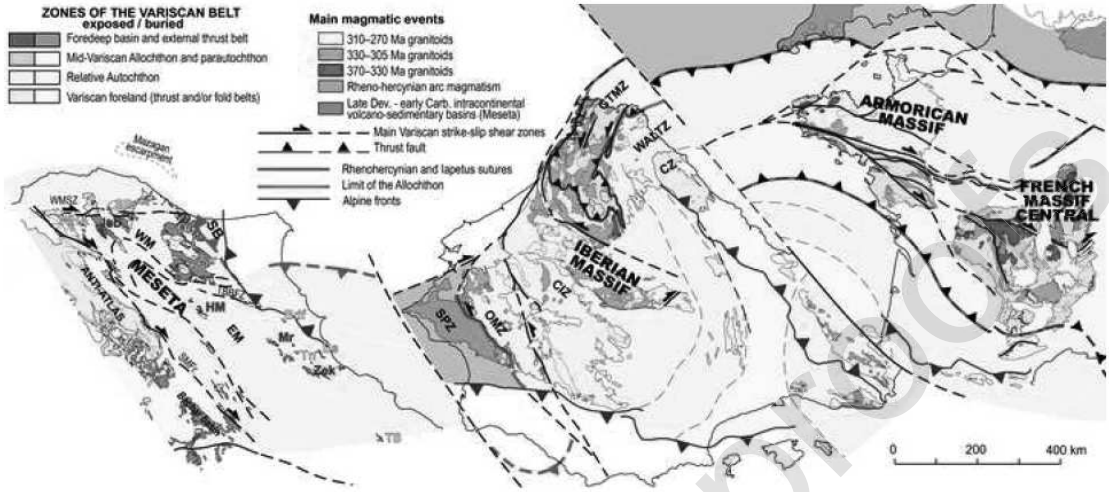

Figure 9

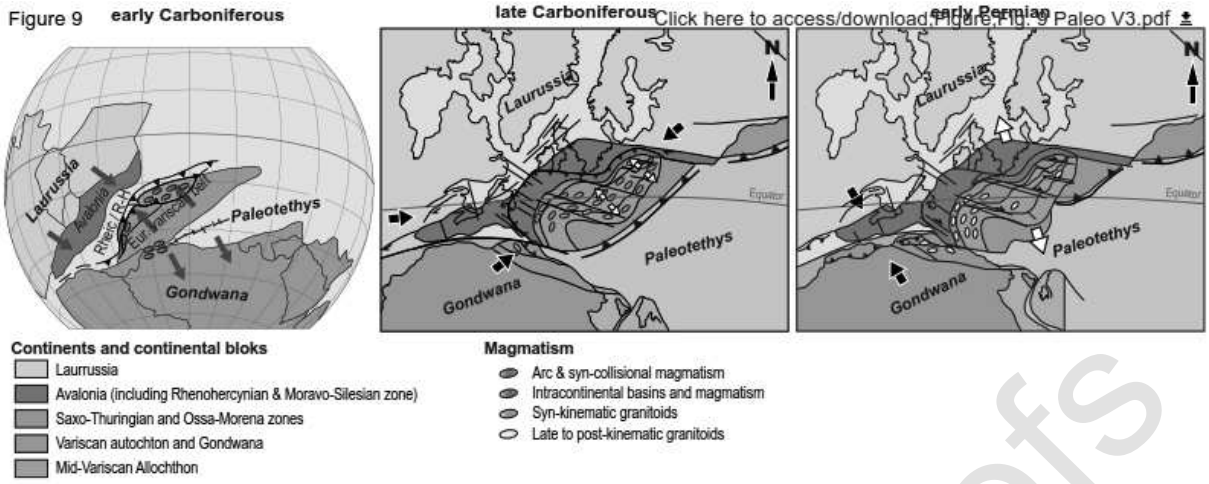

Francis CHOPIN : Conceptualization, Writing - Original Draft, Formal analysis, Investigation, Visualization

Rémi LEPRÊTRE : Conceptualization, Writing - Original Draft, Formal analysis, Investigation, Visualization

Mohamed EL HOUICHA : Writing - Original Draft

Anne-Sophie TABAUD: Writing - Review & Editing, Visualization, Formal analysis,

Karel SCHULMANN : Writing - Review & Editing

Jitka MÍKOVÁ : Formal analysis, Data Curation

Jocelyn BARBARAND : Formal analysis, Data Curation

Ryma CHEBLI : Formal analysis, Investigation

Table 1

Region	Magmatic area/body	Rock type	Age (Ma)	2σ (Ma)	Method and mineral	References
Sehoul Block	Rabat granite	undifferenciated granite	368.7	8	U-Pb Zircon (LA-ICPMS)	Tahiri et al. (2010)
Jebilet	Bamega-Tabouchent	granodiorite	358	7	U-Pb Zircon (LA-ICPMS)	Delchini et al. (2018)
Jebilet	Bamega-Tabouchent	granodiorite	346	10	U-Pb Zircon (LA-ICPMS)	Delchini et al. (2018)
Jebilet	Bamega-Tabouchent	granodiorite	337	4	U-Pb Zircon (LA-ICPMS)	Delchini et al. (2018)
Jebilet	Bamega-Tabouchent	granodiorite	336	4	U-Pb Zircon (LA-ICPMS)	Delchini et al. (2018)
Jebilet	Koudiat Hamra	felsic intrusion	345	2	U-Pb Zircon (LA-ICPMS)	Delchini et al. (2018)
Jebilet	Oulad Ouaslam	granodiorite	348	8	U-Pb Zircon (LA-ICPMS)	Delchini et al. (2018)
Jebilet	Oulad Ouaslam	granodiorite	344	3	U-Pb Zircon (LA-ICPMS)	Delchini et al. (2018)
Jebilet	Oulad Ouaslam	granodiorite	343	7	U-Pb Zircon (LA-ICPMS)	Delchini et al. (2018)
Jebilet	Oulad Ouaslam	granodiorite	337	5	U-Pb Zircon (LA-ICPMS)	Delchini et al. (2018)
Jebilet	Oulad Ouaslam	granodiorite	335.2	0.8	U-Pb Zircon (LA-ICPMS)	This study
Jebilet	Koudiat Kettara	trondhjemite	346.1	2.7	U-Pb Zircon (SHRIMP)	Aït Lahna et al. (2018)
Jebilet	Koudiat Kettara	gabbro	343.6	2.9	U-Pb Zircon (SHRIMP)	Aït Lahna et al. (2018)
Jebilet	Gour es Safra	gabbro	348.5	2.6	U-Pb Zircon (SHRIMP)	Aït Lahna et al. (2018)
Jebilet	Koudiat Arhil	gabbro	336.4	1.6	U-Pb Zircon (SHRIMP)	Aït Lahna et al. (2018)
Jebilet	Koudiat Bouzlaf	microgranitic dyke	330.5	+1.36/−1.66	U-Pb Zircon (ID-TIMS)	Essaifi et al. (2003)
Jebilet	Draa Sfar	rhyolite	330.8	2.2	$^{40}Ar/^{39}Ar$ sericite	Marcoux et al. (2008)
Jebilet	Draa Sfar	rhyolite	331.7	14.8	$^{40}Ar/^{39}Ar$ sericitized plagioclase	Marcoux et al. (2008)
Guemassa	Hajar deposit	sericitized schist	305.4	4.8	$^{40}Ar/^{39}Ar$ hydrothermal biotite	Watanabe (2002)
Guemassa	Hajar deposit	Rhyolite	300.9	2.6	$^{40}Ar/^{39}Ar$ hydrothermal illite	Watanabe (2002)
Rehamna	Lalla Tittaf	metarhyolite	339.5	0.89	U-Pb Zircon (SHRIMP)	Aït Lahna et al. (2018)
Rehamna	Ras el Abiod	microgranitic dyke	285.4	6.1	U-Pb Zircon (ID-TIMS)	Baudin et al. (2003)
Rehamna	Ras el Abiod	mylonitized granite	285.2	5.5	$^{40}Ar/^{39}Ar$ white mica	Chopin et al. (2014)
Rehamna	Nzalet el Hararcha basin	rhyolite	277.07	0.61	U-Pb Zircon (LA-ICPMS)	Domeier et al. (2021)
Rehamna	Mechra Ben Abbou basin	andesite	284.2	4.6	U-Pb Zircon (LA-ICPMS)	Domeier et al. (2021)
Rehamna	Mechra Ben Abbou basin	rhyolite	285.3	4.9	U-Pb Zircon (SHRIMP)	Hadimi et al. (2018) in Domeier et al. (2021)
Rehamna	Sebt Brikiine	granite	274	5.4	$^{40}Ar/^{39}Ar$ biotite	Chopin et al. (2014)
Morocco Central Massif	Oulmès	two micas granite	297	+16/-7	U-Pb Zircon (ID-TIMS)	Baudin et al. (2001)
Morocco Central Massif	Zaër	biotite granite-granodiorite	291	+16/-7	U-Pb Zircon (ID-TIMS)	Chevremont et al. (2001)
Morocco Central Massif	Tiddas Basin	rhyolite	286.4	4.7	U-Pb Zircon (LA-ICPMS)	Hadimi et al. (2021)
Morocco Central Massif	Bou Achouch basin	andesite	301.5	1.24	U-Pb Zircon (LA-ICPMS)	Domeier et al. (2021)
Morocco Central Massif	Chougrane Basin	andesite	295.6 ± 2.9 to 267.9 ± 3.9		U-Pb Zircon (LA-ICPMS)	Domeier et al. (2021)
Morocco Central Massif	Chougrane Basin	andesite	307.8 ± 4 to 295.5 ± 3.4		U-Pb Zircon (LA-ICPMS)	Domeier et al. (2021)
Morocco Central Massif	Khenifra basin	dacite	280.3	2.1	U-Pb Zircon	Youbi et al. (2018) in Domeier et al. (2021)
Morocco Central Massif	Khenifra basin	andesite	282.76	2.19	U-Pb Zircon (LA-ICPMS)	Domeier et al. (2021)
Morocco Central Massif	Khenifra basin	hybrid lavas	287.9	3.8	U-Pb Zircon	Youbi et al. (2018) in Domeier et al. (2021)
Morocco Central Massif	Khenifra basin	rhyolite	290.3	2.1	U-Pb Zircon	Youbi et al. (2018) in Domeier et al. (2021)
Morocco Central Massif	Khenifra basin	pyroclastic lava	290.6	2.6	U-Pb Zircon	Youbi et al. (2018) in Domeier et al. (2021)
Morocco Central Massif	Khenifra basin	dacite	295.1	2.9	U-Pb Zircon	Youbi et al. (2018) in Domeier et al. (2021)
Morocco Central Massif	Khenifra basin	andesite	305.59	2.68	U-Pb Zircon (LA-ICPMS)	Domeier et al. (2021)
Morocco Central Massif	Tighza deposit (Kaolin granite)	biotite-granite	280.6	5.5	$^{40}Ar/^{39}Ar$ igneous biotite	Watanabe (2002)
Morocco Central Massif	Tighza deposit (Ighrem Aouss)	sericitized schist	280.6	3.1	$^{40}Ar/^{39}Ar$ hydrothermal illite	Watanabe (2002)
Morocco Central Massif	Tighza deposit (North veins)	sericitized schist	275.5	3.4	$^{40}Ar/^{39}Ar$ hydrothermal illite	Watanabe (2002)
Morocco Central Massif	Tighza deposit (Mispickel granite)	biotite-granite	267.7	2.3	$^{40}Ar/^{39}Ar$ hydrothermal biotite	Watanabe (2002)
Morocco Central Massif	Tighza deposit (Pb-Zn-Ag deposit)	carbonate gangue	254	16	U-Pb monazite (LA-ICPMS)	Rossi et al. (2016)
Morocco Central Massif	Mine stock (Tighza)	monzogranite	309	10	U-Pb zircon (LA-ICPMS)	Rossi et al. (2016)
Morocco Central Massif	Kaolin stock (Tighza)	monzogranite	295	9	U-Pb zircon (LA-ICPMS)	Rossi et al. (2016)

Morocco Central Massif	Izougarsa stock (Tighza)	monzogranite	295	15	U-Pb zircon (LA-ICPMS)	Rossi et al. (2016)
Morocco Central Massif	Ighrem	microgranite dyke	276	13	U-Pb zircon (LA-ICPMS)	Rossi et al. (2016)
High Moulouya	Perdreaux granite	granite	339.6	1.9	U-Pb Zircon (LA-ICPMS)	This study
High Moulouya	Calco-alcaline «grey» granite	granite	337	1.6	U-Pb Zircon (LA-ICPMS)	This study
High Moulouya	Calco-alcaline «grey» granite	granite	333	2	U-Pb Zircon (ID-TIMS)	Oukemini et al. (1995)
High Moulouya	El Hassir granodiorite	granodiorite	343.1	1.2	U-Pb Zircon (LA-ICPMS)	This study
Horsts belt	Zekarra	granodiorite	348.1	2.3	U-Pb Zircon (LA-ICPMS)	This study
Horsts belt	Merguechoum	granite	345.2	2.8	U-Pb Zircon (LA-ICPMS)	This study
Horsts belt	Beni Snassene	monzogranite	308.2	2.7	U-Pb Zircon (LA-ICPMS)	This study
Horsts belt	Tanncherfi	granodiorite	303.5	1.7	U-Pb Zircon (LA-ICPMS)	This study
Horsts belt	Boudoufoud	granite	305.2	1.4	U-Pb Zircon (LA-ICPMS)	This study
Algerian High Plateaux	Trifrit/Saïda	granodiorite	297	1	U-Pb Zircon (ID-TIMS)	Remaci-Benaouda (2005)
Western High Atlas	Azegour	granite	275.6	3.4	U-Pb Zircon (SHRIMP)	Ettachfini et al. (2018)
Western High Atlas	Azegour	rhyolite	279	2.6	U-Pb Zircon (SHRIMP)	Ettachfini et al. (2018)
Western High Atlas	Azegour	microgranite	283	3	U-Pb Zircon (SHRIMP)	Ettachfini et al. (2018)
Western High Atlas	Bouzouga	granite	279	1.8	U-Pb Zircon (SHRIMP)	Fekkak et al. (2018)
Western High Atlas	Tawrirt	granite	295	3	U-Pb Zircon (SHRIMP)	Fekkak et al. (2018)

Table 1: Compilation of U-Pb and $^{40}Ar/^{39}A$ ages of magmatic rocks and deposits from the Meseta